8-2008

Evaluation of a New Method to Estimate the Micropore Volume and External Surface Area of Single-walled Carbon Nanotubes

Yijing Zheng
University of Tennessee - Knoxville

To the Graduate Council:

I am submitting herewith a thesis written by Yijing Zheng entitled "Evaluation of a New Method to Estimate the Micropore Volume and External Surface Area of Single-walled Carbon Nanotubes." I have examined the final electronic copy of this thesis for form and content and recommend that it be accepted in partial fulfillment of the requirements for the degree of Master of Science, with a major in Environmental Engineering.

Sandeep Agnihotri, Major Professor

We have read this thesis and recommend its acceptance:

Chris D. Cox, Terry L. Miller, David J. Keffer

Accepted for the Council:
Carolyn R. Hodges

Vice Provost and Dean of the Graduate School

(Original signatures are on file with official student records.)

To the Graduate Council:

I am submitting herewith a thesis written by Yijing Zheng entitled “Evaluation of a New Method to Estimate the Micropore Volume and External Surface Area of Single-walled Carbon Nanotubes.” I have examined the final electronic copy of this thesis for form and content and recommend that it be accepted in partial fulfillment of the requirement for the degree of Master of Science, with a major in Environmental Engineering.

Sandeep Agnihotri

Major Professor

We have read this thesis
and recommend its acceptance:

Chris D. Cox

Terry L. Miller

David J. Keffer

Accepted for the Council:

Carolyn R. Hodges

Vice Provost and Dean of the
Graduate School

(Original signatures are on file with official student records.)

Evaluation of a new method to estimate the micropore volume and external surface area of single-walled carbon nanotubes

A Thesis

Presented for the

Master of Science

Degree

The University of Tennessee, Knoxville

Yijing Zheng

August 2008

ACKNOWLEDGEMENTS

I would like to express my sincere gratitude and appreciation to my advisor Dr. Sandeep Agnihotri, for his guidance and encouragement during my time at the University of Tennessee. My appreciation is also extended to the members of my committee, Dr. Chris D. Cox, Dr. Terry L. Miller and Dr. David J. Keffer for their support and constructive criticism of my work.

Special thanks go to Dr. Harry M. Meyer of Microscopy Group at Oak Ridge National Laboratory, for his assistance in some of my experimental work.

I wish to thank my best friend Dan Zhao and Jidong Xu, for helping me get through the difficult times, and for all the emotional support, entertainment, and caring they provided.

Special thanks go to Patrick Cai for proof reading this thesis and giving much support and encouragement.

Last but not the least, I would like to thank my dearest parents and family in China for their endless love and unconditional support. This thesis is dedicated to Mr. Youjun Zheng and Mrs. Ping Li.

ABSTRACT

Since the discovery of carbon nanotubes in 1991, significant progress has been made to understand their electrical, mechanical, magnetic and optical properties. However, as the ideal adsorbent for adsorption of gases and vapors, nanotubes, especially the single-walled carbon nanotubes (SWNTs), and their adsorption properties remain not been investigated enough. The unique microporous structure of SWNTs gives them remarkable adsorption properties, i.e. surface area and porosity. Several methods exist to determine the surface area and pore volume of adsorbents: t-plot method, Dubinin-Radushkevich (DR) method, and Dubinin-Astakhov (DA) method. The results are usually specific to a certain method and to the segment of the adsorption isotherm which is fitted to the method used. Therefore, the main objective of this study is to find the most appropriate and suitable method to characterize micropore volume and external surface area of SWNTs.

The surface area and porosity results are often used to evaluate the effectiveness of an adsorbent for removal of odors and trace concentrations of organic vapors from air and process streams. The objective is accomplished by evaluating the results of t-plot method, DR method, DA method and a method that was recently developed. Some of the commonly used methods were developed as far back as 1940s. Additionally, the methods were developed for various adsorbents such as carbon black, zeolites and

activated carbon. However, nanotubes are fairly recent adsorbent materials. All of these can render the characterization results open to the interpretation by a specific user.

In this study standard N_2 adsorption was carried out at 77 K for four commercially available SWNT sample. The impurities of SWNTs were able to be incorporated into the adsorption isotherm, the results of which could be confirmed by thermogravimetric analysis (TGA) and X-ray photo spectroscopy (XPS) experiments. To make the new developed method applicable to impure SWNT samples, new definition of statistical thickness has been proposed in this study. The consistent results showed the advantages of the modified new method, which is applicable and specific to SWNT samples. Multiple adsorbates should be used in the future analysis, such as water vapor, hexane, and other organic vapors.

TABLE OF CONTENTS

LIST OF TABLES

LIST OF FIGURES

Chapter 1

INTRODUCTION

1.1 Carbon Nanotubes

Since carbon nanotubes were first discovered by Iijima[1] in 1991, an extensive research has been dedicated to this new material. Atomically, the structure of carbon nanotubes resembles that of a rolled up graphite sheets, with an inner diameter starting from 0.7 nm to several nanometers (nm) and a length ranging from 10's nm to 10's μm. Carbon nanotubes can be either single-walled (SWNTs), which are formed by only one single graphite layer, or multi-walled carbon nanotubes (MWNTs), which has two or more graphite layers rolled together with a common axis to form concentric SWNTs. Figure 1.1 and 1.2 show the structure of SWNT and MWNT, while Figure 1.3 is the schematic diagram of SWNT and grapheme layer. Unlike MWNTs, the atoms of SWNTs form a single covalently bond array. Thus SWNTs have more distinctive electrical and optical properties when compared to MWNTs. Typically, the diameter of SWNT is around 1.2-1.4 nm and the length ranges from 10's nm to 10's μm[2]. SWNTs are always found in rope-like bundles. They are one of the most commonly researched nanomaterials due to their exceptional mechanical, electrical and thermal properties[3, 4]. Carbon nanotubes have been used for developing biosensors[5], gas storage devices[6], and removal of hazardous pollutants from gas stream[7, 8].

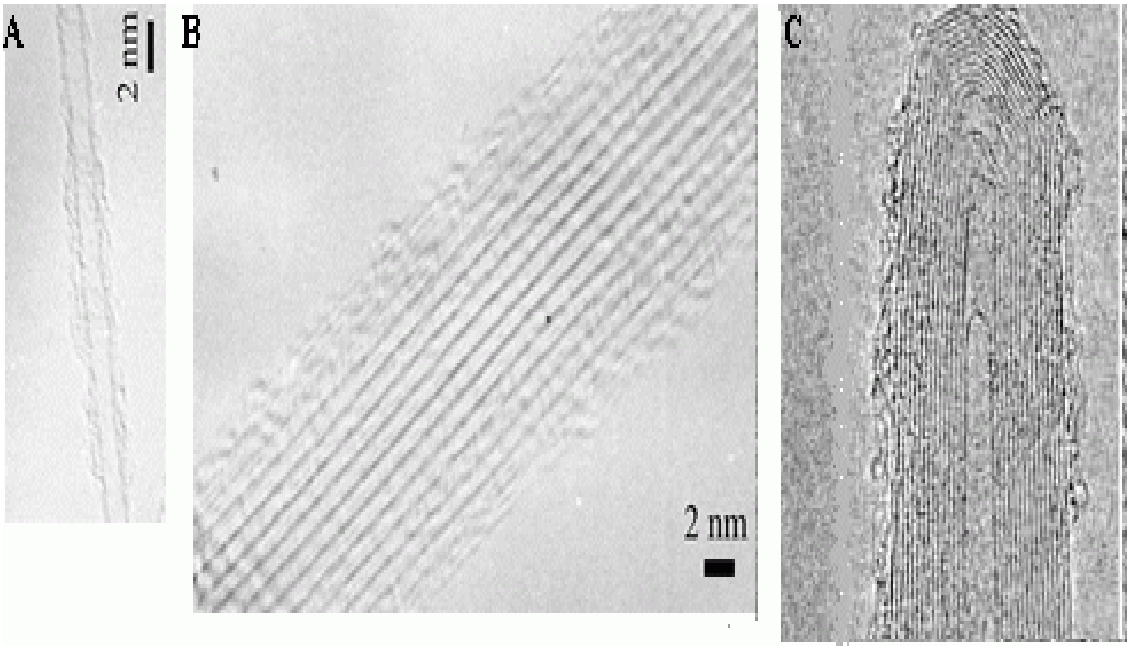

Figure 1.1. High resolution Transmission Electron Microscopy (TEM) images of (A) isolated SWNT, (B) SWNT bundles, and (C) MWNTs[9].

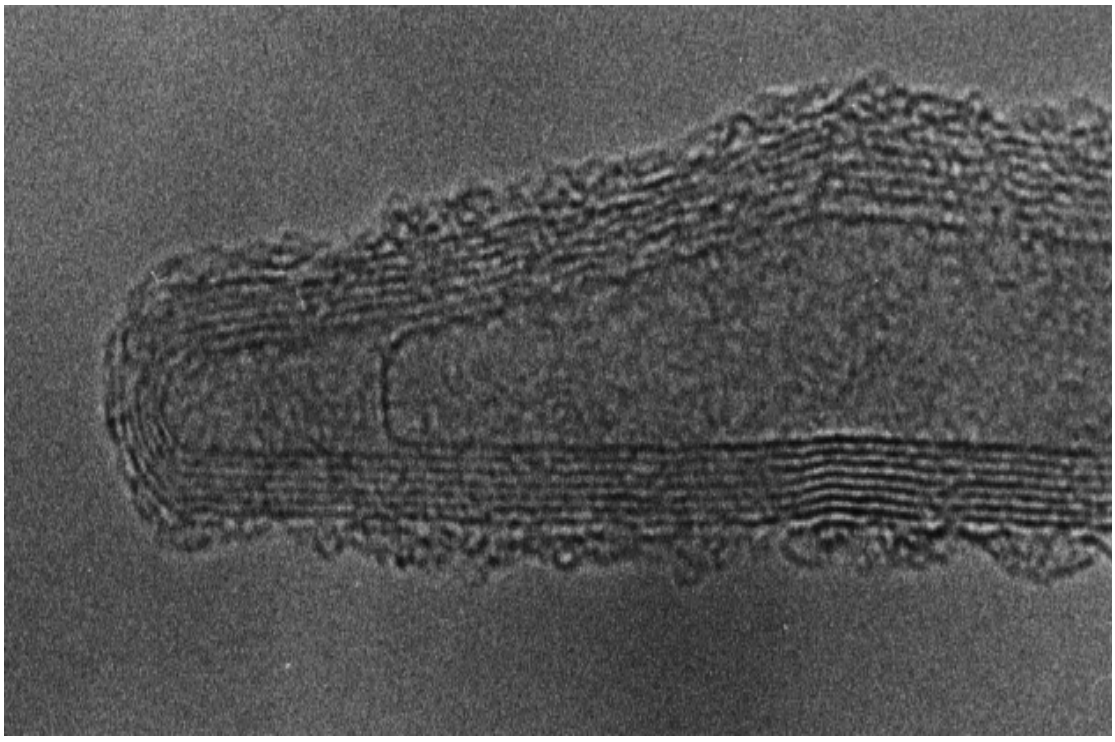

Figure 1.2. TEM image showing typical carbon nanotube in the tip region[10].

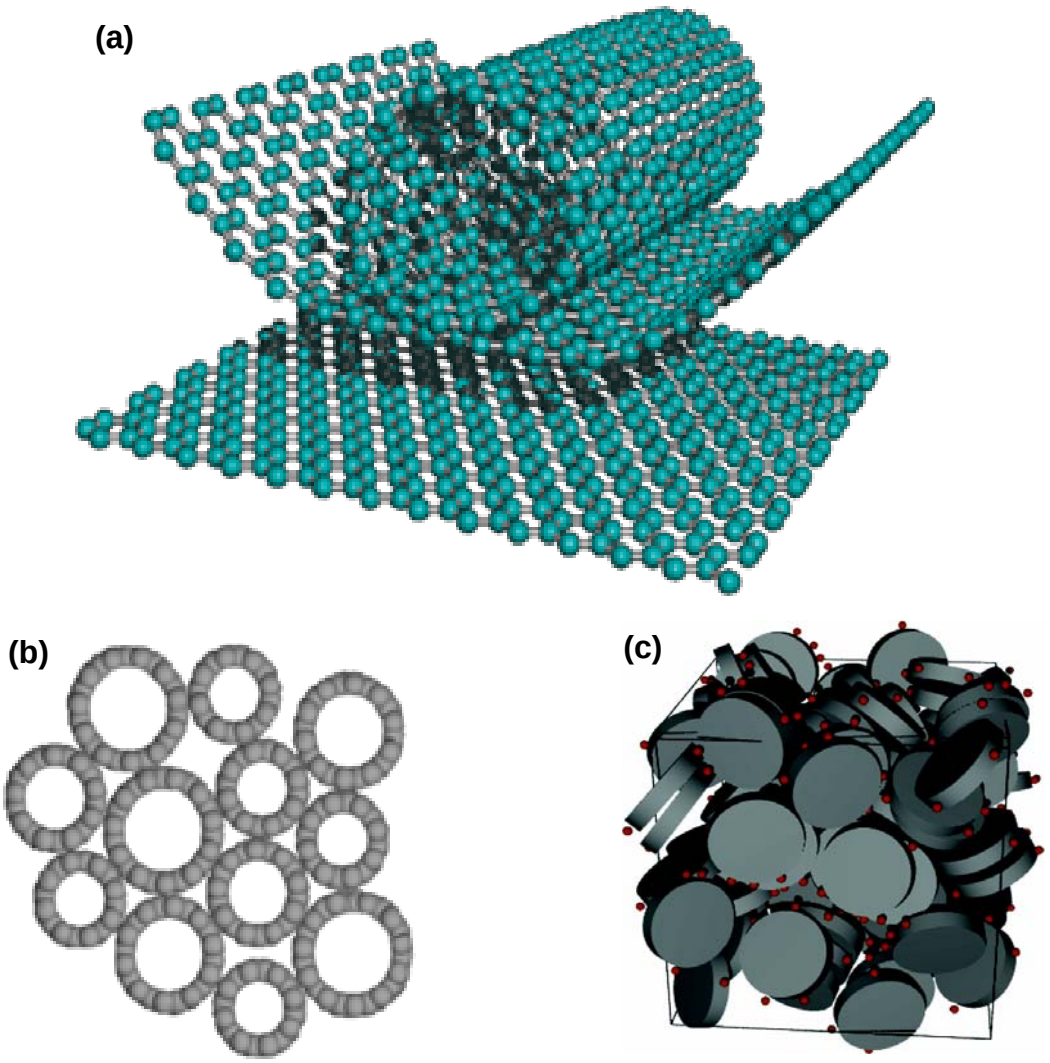

Figure 1.3. Schematic diagrams of (a) graphene layer, i.e., individual carbon layer in the honeycomb graphite lattice, which could be rolled up to form a carbon nanotube (CNT)[11], (b) heterogeneous bundles of SWNT[12], and (c) activated carbon, of which each cluster is a stack of graphene layers[13].

1.2 Environmental Studies of Carbon Nanotubes

The application of carbon nanotubes in environmental field has been evaluated recently. Researchers in this field have focused mainly on the use of carbon nanotubes as a novel adsorbent for gases and vapors. Following is a brief review of relevant studies.

Ohno *et al*. (2006)[14] investigated the environmental effects on photoluminescence of SWNTs by using air-suspended SWNTs and sodium-dodecyl-sulfate (SDS)-wrapped SWNT samples. Compared to the SDS-wrapped SWNTs, the optical transition energy E_{11} and E_{22} of the air-suspended SWNTs showed blueshifts. Only the E_{22} of the near-zigzag type SWNTs were found to show redshifts. Yu *et al*. (2008)[15] treated the SWNTs with sulfuric acid at 300^{o}C to synthesize sulfonated SWNTs (s-SWNTs). They characterized s-SWNTs and found that the high degree of surface sulfonation could transform the hydrophobic surface of SWNTs into a hydrophilic surface. This made s-SWNTs stable and uniformly dispersed in water and organic solvents. These authors suggested that water-dispersive functionalized SWNTs can be used as an environmentally relevant catalyst. Jeong *et al.*(2007)[16] reported size control of catalytic nanoparticles and found that thinner SWNTs with a narrower diameter distribution grew as the nanoparticles became smaller. The results provided a straightforward technique to prepare catalysts that have a desirable size and

uniformity towards diameter-controlled growth of SWNTs.

Chen *et al*. (2007)[17] evaluated the adsorption of organic compounds of varying physical and chemical properties onto SWNT and MWNT samples. They assessed the potential impact of carbon nanotubes on the fate and transport of organic contaminants in the environment. They concluded that the adsorption affinity correlated poorly with hydrophobicity; however, it increased in the order of nonpolar aliphatic < nonpolar aromatics < nitroaromatics, and it increased with the number of nitrofunctional groups within the group of nitroaromatics. Yuan *et al*. (2006)[18] prepared capillary columns using SWNTs, ionic liquid (IL), and IL+SWNTs for gas chromatography (GC). The separation results showed that SWNTs possessed a broad selectivity toward alkanes, alcohols, aromatic compounds, and ketones. Compared to other two capillary columns, a SWNT capillary column was a very useful GC column for the separation of gas samples. Kang *et al*.(2007)[19] explored the application of SWNT as building blocks for antimicrobial materials. They found that direct cell contact with highly purified, pristine SWNTs with a narrow diameter distribution can cause severe membrane damage. Their finding provided the first direct evidence that highly purified SWNTs exhibit strong antimicrobial activity.

1.3 Adsorption Properties of Carbon Nanotubes

Separation and adsorption processes are one of the most common environmental processes. Therefore, in order to find applications of carbon nanotubes (CNTs) for the environment, concepts of adsorption on CNTs need to be identified first. There are two types of adsorption mechanisms: physical and chemical adsorption. Physical adsorption is also referred to as physisorption. It is caused by molecular interactions due to van der Waals forces between the adsorbate molecules and the adsorbent surface. On the other hand, chemical adsorption is essentially a chemical reaction which includes the formation of covalent bonds between the adsorbate and the molecules on the surface of the adsorbent. Chemical adsorption is also referred to as chemisorption. The concepts of adsorption on carbon nanotubes discussed here forth are defined for physisorption.

Hollow space structured CNTs provide two types of adsorption sites: inner and outer, which are also defined as internal site and external site. The internal site is only accessible when the carbon nanotubes are open-ended [20], while the external adsorption site is available unconditionally. However, the tips of CNTs are often found closed for both SWNTs and MWNTs. Since, SWNTs exist in bundles, the adsorption sites are defined for the entire bundle as opposed to an individual nanotube. This is one of the most important distinctions between SWNTs and MWNTs.

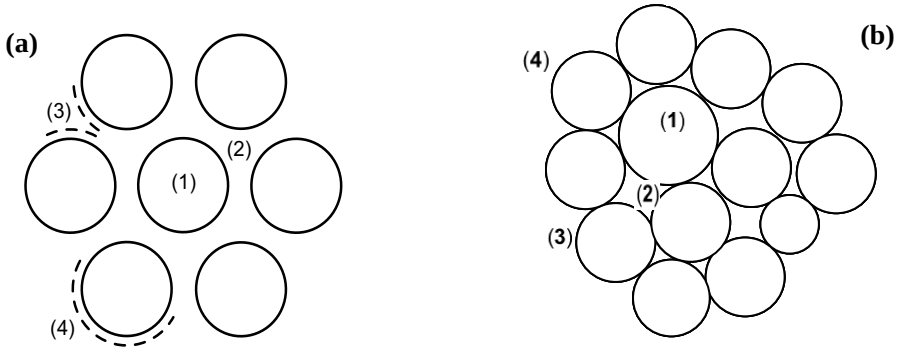

Figure 1.4. Four specific adsorption sites on (a) homogeneous bundles, and (b) heterogeneous bundles of SWNTs[21].

Adsorption on SWNTs typically occur on four sites, which are (1) internal volume of nanotubes, (2) interstitial channels between two or more adjacent nanotubes, (3) grooves sites on the external layer of nanotube shell, and (4) the external surface of the outermost nanotubes in the bundle. Figure 1.4 shows[21] all these four adsorption sites on either homogeneous or heterogeneous bundles of SWNTs. Adsorption on the external surface area of SWNTs only occurred when the internal sites are saturated with adsorbate molecules.

As a relatively new adsorbent, the pore volume and surface area of SWNTs needs to be evaluated. SWNTs have a unique microporous structure. Micropores are defined as pores of width less than or equal to 2 nm[22]. This microporous structure gives SWNTs remarkable adsorption properties. Several methods exist to determine the surface area and pore volume of adsorbents. The most commonly used methods include t-plot method, Alpha-s (α_s) method, MP method, Dubinin-Radushkevich (DR)

method, and Dubinin-Astakhov (DA) method. The estimated micropore volume is usually specific to a certain method and to the segment of the adsorption isotherm which is fitted to the method used. Theoretically the surface area of SWNTs could be reached as high as 3,000 m^2/g[23]. But the reported surface area of carbon nanotubes ranges from 150 to 1,587 m^2/g, which is far lower than the theoretical value[24]. It is known that the porosity and surface area results of carbon nanotubes are usually specific to a particular study and are not easily replicable by other researchers. The reported surface area of SWNTs varies greatly. It depends on the adsorbate gas used for adsorption, the specific structure and composition of SWNT samples tested, and the estimated methods used in the porosity and surface area analysis.

1.4 Objectives and Significance

The evaluation of carbon nanotubes as an adsorbent in the environmental field, such as to develop nanoscale sensors to detect air pollutants[25], to remove hazardous air pollutants and other contaminants from gas streams[7, 8] has been attracting a lot of attention in the recent years. Adsorption properties of carbon nanotubes need to be evaluated to understand how best to apply carbon nanotubes for environmental engineering. The pore volume and surface area are the two main characteristics that indicate the adsorption capacities of an adsorbent. The traditional characterization methods, such as t-plot method, may not be applicable to the more novel materials

such as nanotubes which are more structured than other common carbon adsorbents such as activated carbons. Thus finding a method to accurately estimating the micropore volume and external surface area of SWNTs is important to develop a better understanding of the applications and limitations of carbon nanotubes.

The objective of this study is to find the most appropriate and suitable method to characterize adsorption micropore volume and external surface area of SWNTs. These properties are often used to evaluate the effectiveness of an adsorbent for removal of odors and trace concentrations of organic vapors from air and process streams. The objective is accomplished by evaluating the results of several common characterization methods[26, 27] and a method that was recently developed[21].

As an example, the t-plot method is one of the most common characterization methods. The method requires estimating the thickness of an adsorbate layer, such as that of N_2 molecules, from the isotherm data collected. The thickness of the adsorbate layer is typically referred to as the statistical thickness, *t*. Plotting the adsorption capacities versus *t* yields a straight line. The intercept and slope of such a straight line, respectively, represents the micropore volume and the external surface area of the adsorbent. The present study evaluated the pore volume and surface area of several SWNTs by calculating their values using common methods and a newly developed method.

Some of the commonly used methods were developed as far back as 1940s. Additionally, the methods were developed for various adsorbents such as carbon black, zeolites and activated carbon. However, nanotubes are fairly recent adsorbent materials. Although a carbonaceous material, the atomic structure of nanotubes is much different from that of carbon black and activated carbons. The atomic structure of nanotubes might also induce adsorption forces that can not be explained by traditional models such as the t-plot method. Furthermore, the characterization results of these models also depend upon the segment of the experimental adsorption isotherm that is selected for data fitting. This can render the characterization results open to the interpretation by a specific user.

Therefore, the applicability of these methods to new materials, such as carbon nanotubes, needs to be evaluated. This is attempted here. In this study standard N_2 adsorption was carried out at 77 K and the impurities of SWNTs were able to be incorporated into the adsorption isotherm, the results of which could be confirmed by thermogravimetric (TGA) experiments.

Chapter 2

METHODOLOGY

2.1 Experimental Methods

2.1.1 Sample Information

For this study, SWNT samples were selected based on two different synthesis methods: electric-arc (EA) and chemical vapor deposition (CVD)[20], which should provide a comprehensive data set to delineate effects of SWNT sample morphologies, if any. The EA produced SWNT samples were purchased from MER Corporation in Tucson, AZ and Carbon Solutions Inc. in Riverside, CA. The samples are referred to as *EA95* and *CS70* respectively, where 95 and 70 represents 95 wt% and 70 wt% SWNTs, respectively, as characterized by the sample manufacturer. The CVD process uses high pressure (up to 10 atm) carbon monoxide with Fe catalyst particles. This process is now commonly known as the HiPco process. The HiPco SWNT samples were purchased from Carbon Nanotechnologies Inc in Houston, TX. Here, the sample is referred to as *CVD95*. It contains > 95 wt% of SWNTs and small amount of Fe catalyst. Another SWNT sample used in this study is *BU90*, of which the SWNT percentage is around 90 wt%, purchased from Bucky USA.

2.1.2 Physical Characterization of Samples

2.1.2.1 Methodology for Quantachrome Surface Area Analyzer

The standard N_2 adsorption isotherms at 77 K were obtained by using an Autosorb-1-C Chemi-Physisorption Surface Area Analyzer (Quantachrome Instruments). The instrument is located in 702 Science and Engineering Facility (SERF) of the University of Tennessee (Figure 2.1). This instrument is fitted with a 1 Torr transducer which allows accurate adsorption measurements at as low as 10^{-6} P/P_o. Here, P is the actual vapor pressure of N_2 and P_o is the saturation vapor pressure of N_2 at 77 K (= 760 torr). For each run, 25-30 mg of SWNT sample was used.

Figure 2.1. Quantachrome Autosorb-1-C

The operation procedure consists of two steps: outgassing and physisorption analysis. To start a new run, the SWNT sample was first outgassed at 140 ^{o}C under 1 millitorr vacuum for a continuous 24 hours period of time. This outgassing step cleans and prepares the sample for collection of adsorption data. After this step, the sample is then cooled down to 77 K by liquid N_2. A predetermined set of relative vapor pressure (P/P_o) values is fed to the instrument by the control panel interface. The instrument computer then doses the sample cell with those predetermined gas pressures and estimates equilibrium adsorption by volumetric conversions of the loss in gas pressure in the sample cell. The adsorption isotherms are obtained in the relative pressure range of $10^{-6} < P/P_o < 0.99$.

2.1.2.2 Methodology for TGA

Thermogravimetric technique was used to evaluate the purity of some of the SWNT samples tested in this study. In order to determine the quantity of impurities in the samples, the experiments are performed using as the carrier gas laboratory grade air which oxidized the carbon but left the impurities as ash. The thermogravimetric analysis was performed using the Perkin-Elmer TGA Pyris 1 instrument. It is located at the Forest Products Center in the College of Agriculture of the University of Tennessee at Knoxville (Figure 2.2).

Figure 2.2. Perkin-Elmer TGA Pyris 1

Thermogravimetry is a method to measure the sample weight as a function of temperature. In a typical experiment, the SWNT sample CS70 (6.898 mg) was loaded in a platinum pan that was enclosed in a vertical electric furnace for weight loss measurement. The sample was heated in air at a constant ramping rate of 20 ^{o}C/min from room temperature to up to 900 ^{o}C. Laboratory grade air with 20 ml/min flowrate was used as carrier gas. At 900 ^{o}C, the temperature was held constant for 10 min to minimize the fluctuation of the weight change of sample due to temperature changes. Once the temperature was stable at 900 ^{o}C, the furnace was turned off and the sample was cooled from 900 ^{o}C to room temperature. The last step was to keep the furnace and the burned sample ash under room temperature for 10 hours. During the entire operation the instrument computers monitors and stores the sample weight,

temperature and time data for analysis after the run is complete.

It is to be noted that during a TGA operation, the increase of temperature reduces the density of the carrier gas surrounding the sample. This changes the buoyant forces experienced by the sample which can introduce incorrect weight changes as an artifact of the operating procedure. Such effects can seriously misrepresent TGA information, especially for samples used in very small quantities as in this study. Here, we counteracted the buoyancy effects by operating the TGA with an empty pan under exact same gas flow rate and temperature and other operating parameter conditions. This created a blank data set as a reference line against which all TGA data sets were re-scaled.

It is also to be noted that after the TGA run is completed, the quantity of ash left in the sample pan may not be a true indicator of the impurities in the test samples. This is because the normal TGA operation raises the sample temperature high enough that it can also oxidize the pure metal catalyst impurities in samples. For example, Fe oxides to Fe_2O_3 at 600 to 700 ^oC which is within the operating temperature range; therefore, a nanotube sample containing Fe metal catalyst would leave a reddish brown ash. Here, such oxidation effects were also taken in the impurity analysis from TGA.

2.1.3 Chemical Characterization of Samples

2.1.3.1 Methodology for Raman Spectroscopy

Raman spectroscopy is a nondestructive light scattering technique. It requires the sample to be placed in the path of an excitation beam. It collects the scattered light. It is very powerful tool that is often used to investigate the modifications in the atomic arrangements of carbon nanotubes, especially SWNTs. In the use of Raman spectroscopy, the photon excites one of the electrons into a virtual state. When the photon is released the molecule relaxes back into its original vibrational energy state. Raman scattering is only a small fraction of the scattered light, which is about 1 in 1 million photons. Most of the photos scattered as Rayleigh scattering (black line with arrow in Figure 2.3). The molecule will typically relax into the first vibrational energy state, and this generates Stoke Raman scattering (green line with arrow in Figure 2.3). If the molecule was already in an elevated vibrational energy state, the Raman scattering is then called Anti-Stokes Raman scattering (purple line with arrow in Figure 2.3). In the experiment of Raman spectroscopy, the change of the molecular polarizability could be used to determine the intensity of Raman scattering (Y – axis of spectra), and the Raman shift (X – axis of spectra) is equal to the vibrational level that is involed[28].

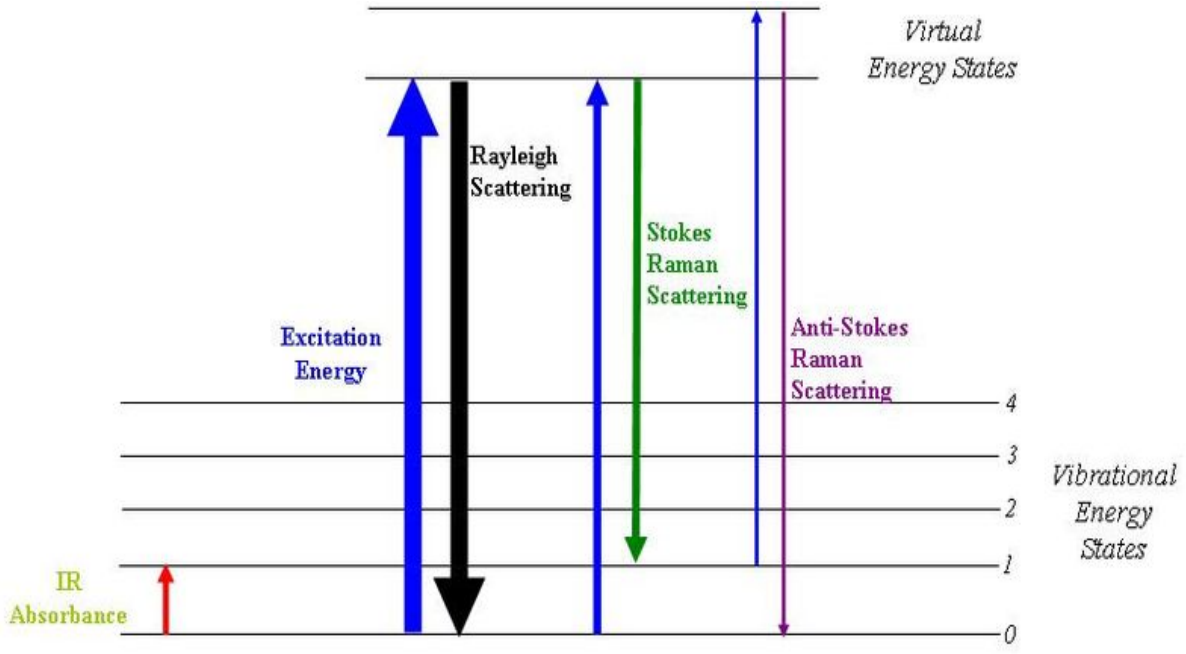

Figure 2.3. Energy level diagram showing the states involved in Raman signal. The line thickness is roughly proportional to the signal strength from the different transitions[28].

Raman spectroscopy can be used to determine the diameter of nanotube[29] and explore the electronic structure of nanotubes[30]. There are four important features in typical Raman spectra of a SWNT sample: radial breathing mode (RBM) peaks, D-peak, G-peak, and G'-peak. Among all of these four kinds of peaks, RBM peaks, which frequencies are in the range of 100-300 cm^{-1}, provide information about the diameter and chirality of nanotubes. The relation between RBM frequency of nanotube and the diameters of the sample is denoted as this equation:

$$\omega_{RBM} = 12.5 + \frac{223.5}{D(nm)} \quad (1)$$

where ω_{RBM} is the RBM frequency, $D(nm)$ is nanotube diameter with the unit of nanometer.

It is known that Raman scattering by single excitation energy may not be sufficient to explore all of the SWNT diameters. In this study, multiple excitation energies of Raman scattering were used on all of the four samples tested at $\lambda = 532$ nm and $\lambda = 633$ nm (T6400 Raman research system by JY Horiba, and Renishaw 100 MicroRaman System, respectively). Besides, single excitation energy of Raman scattering experiments at $\lambda = 785$ nm were performed on SWNT EA and HiPco samples in the previous research[21] using NXR FT-Raman (Figure 2.4). The instrument is located in 702 Science and Engineering Facility (SERF) of the University of Tennessee.

Figure 2.4. NXR FT-Raman Module

2.1.3.2 Methodology for X-ray Photospectroscopy

X-ray photoelectron spectroscopy (XPS) is a surface chemical analysis technique. It is very sensitive to the composition and chemical bonding states of materials. XPS analyses were carried out by Perkins-Elmer XPS and Thermo K-Alpha XPS (Figure 2.5). The instrument is located at High Temperature Materials Laboratory (TEML) in Oak Ridge National Laboratory (ORNL). Thermo K-Alpha XPS at TEML is the second model being used in the world, whereas the first K-Alpha XPS came out and being used by National Aeronautics and Space Administration (NASA). The spectra were collected using the 04-548 Dual Anode (Mg/Al) Kα X-ray source; at an 89.45 eV pass energy and at a power of 300 W, 15 kV. The base pressure of the system was normally maintained below 10^{-9} Torr.

Figure 2.5. Thermo K-Alpha XPS located at Oak Ridge National Laboratory.

2.2 Estimating Micropore Volume & Surface Area

2.2.1 Common Methods

Estimate micropore volume and surface area using common methods, e.g. t-plot method, DR method, and DA method, standard N_2 adsorption experiments have been performed by Quantachrome Autosorb-1-C equipment. It could generate a whole adsorption isotherm after each run. After that Quantachrome built-in software could be used to analyze the data by selecting different microporosity analysis methods, e.g. t-plot method, DR method and DA method for this study.

2.2.1.1 t-plot Method

The *t-plot* method is one of the most commonly used methods to determine (external) surface area and pore volume of an adsorbent. This method requires estimating the thickness of an adsorbate layer, such as N_2, as a function of relative pressure (P/P_o). It is typically referred to as the statistical thickness, *t*. Typically, the *t* values are calculated using one of the three equations: de Boer equation[26] (Eq. 2), Carbon Black equation[31] (Eq. 3), and the Halsey equation[32] (Eq. 4).

$$t(\overset{o}{A}) = \left[\frac{13.99}{0.034 - \log(P/P_o)}\right]^{1/2} \quad (2)$$

$$t(\overset{o}{A}) = 0.88\,(P/P_o)^2 + 6.45\,(P/P_o) + 2.98 \quad (3)$$

$$t(\overset{o}{A}) = 3.54\left[\frac{5}{2.303\log(P_o / P)}\right]^{1/3} \quad (4)$$

It is to be noted that the numerals in equations (2) to (4) are optimized for N_2 adsorbate. Using inert gases other than N_2, such as Ar, Kr and CO_2, would require different numeral values in these equations.

In order to determine with sufficient accuracy pore volume and surface area values using t-plot method, two criteria need to be employed: (i) selecting one of the abovementioned Eq. (2) to (4), and (ii) selecting adsorption values corresponding to an appropriate range of relative pressure from the total isotherm data collected by the instrument. The de Boer equation (Eq, 2) was developed for well-selected samples of alumina; however, it is applicable to other materials including graphitized carbon blacks[31]. Carbon Black and Halsey equations (Eq. 3 and 4) are applicable to carbon black and related materials. It was reported that the relative pressure range for the Carbon Black equation (Eq. 3) is $0.2 < P/P_o < 0.5$[31]. However, there is no specific relative pressure range reported for de Boer and Halsey equation. The procedure of t-plot method is the same as that employed in the multi-point Brunauer-Emmett-Teller (BET) surface area[33] measurement. Therefore, in the determination of micropore volume and surface area by t-plot method, the relative pressure range should be chosen same as that used in the BET surface area measurement. Equation (5) is the multi-point BET equation.

$$\frac{1}{W\left(\left(P_0 / P\right)-1\right)} = \frac{1}{W_m C} + \frac{C-1}{W_m C}\left(\frac{P}{P_0}\right) \tag{5}$$

Where W is the weight of gas adsorbed at a relative pressure, P/P_0, and W_m is the weight of adsorbate constituting a monolayer of surface coverage. The term C, the BET C constant, is related to the energy of adsorption in the first adsorbed layer.

By plotting $1/[W(P/P_0)-1]$ versus P/P_0, it could generate a linear curve, usually in the limited relative pressure range of 0.05 to 0.35, using nitrogen as the adsorbate. The weight of a monolayer of adsorbate W_m can be obtained from the slope and intercept of the BET linear plot. Therefore, in this study we used the relative pressure region of $0.05 < P/P_o < 0.35$ for both de Boer and Halsey equation and $0.2 < P/P_o < 0.5$ for Carbon Black equation in the determination of surface area of SWNTs when using t-plot method.

In the t-plot, the adsorption capacity ([STP]/g) is plotted as the ordinate and the statistic thickness, t (nm), is plotted as the abscissa (Figure 2.6). Typically, the t-plot yields a straight line. The intercept and slope of the straight line are interpreted as the micropore volume and the external surface area, respectively, according to the following relations.

$$V_{MP} = i \times 0.001547(cm^3) \tag{6}$$

$$S_t\left(m^2 / g\right) = 15.47 \times s \tag{7}$$

where i is the intercept (cm^3[STP]/g), s is the slope of the straight line fitted to the t-plot, and the constant 15.47 represents the conversion of the gas to liquid volume.

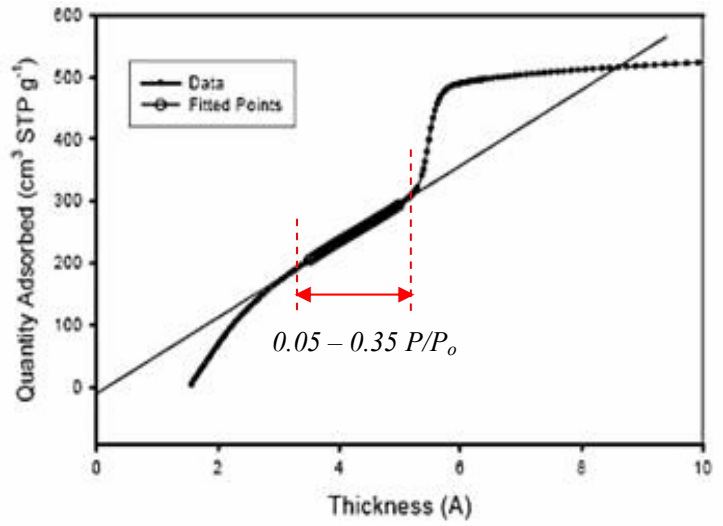

Figure 2.6. Illustration of t-plot method to calculate pore volume and surface area[34]. The isotherm data points fitted a linear curve in the relative pressure range of 0.05 < P/P_o < 0.35 (showed in red).

In this research, the t-plot method was applied to the Autosorb data collected for four SWNT samples: EA95, CVD95, CS70, and BU90, which has >95 wt%, > 95 wt%, 70 wt%, and 90 wt% of purity, provided by the manufacturer.

2.2.1.2 DR Method

DR method, developed on the basis of Polanyi potential theory of adsorption[35], was proposed by Dubinin and Radushkevich (DR)[27] in 1947. It was first developed for adsorption analysis on homogeneous microporous activated carbons. They assume that the fraction of adsorption volume, *W*, occupied by liquid adsorbate, e.g., nitrogen, at various adsorption potentials ε could be expressed as a Gaussian function[36],

$$W = W_0 \exp\left[-\left(\frac{A}{\beta E_0}\right)^2\right] \tag{8}$$

where *A* is the free energy of adsorption, *W* and W_0, respectively, are current and limiting micropore volumes for adsorption per unit mass of adsorbent (cm^3/g), E_0 is the characteristic adsorption energy of the reference adsorbate (usually benzene), and β is the affinity coefficient. In Dubinin's early paper *A* was called adsorption potential ε,

$$A = \varepsilon = -\Delta G = RT \ln(P_0 / P) \tag{9}$$

The coefficient β can be approximated as a ratio of the liquid molar volumes v of a given adsorbate, e.g., nitrogen and benzene, which is used as the reference liquid[37],

$$\beta = \frac{v}{v_{C_6H_6}} \tag{10}$$

Thus equation (8) can be written in the linear form,

$$\log W = \log(W_0) - 2.303\left(\frac{RT}{\beta E_0}\right)^2 \log(P_o / P)^2 \tag{11}$$

The slope and intercept of the linear plot, $\log(W)$ versus $\log(P_o / P)^2$, can be used to obtain characteristic free energy E_0 and micropore volume W_0. Kaganer[38] used this linear plot to evaluate micropore surface area by the intercept, $\log(W_0)$. It has been found that the linear range of this plot appears at relative pressures (P/P_o) less than 10^{-2}. The slope, *m*, of the linear fitted straight line equals to $-2.303\left(\frac{RT}{\beta E_0}\right)^2$ while the intercept is $\log(W_0)$. To get a better data fit for non-Gaussian pore size distributions, Dubinin[39] pointed out that the DR exponent, *n*, could be differed from *n* = 2.

2.2.1.3. DA Method

Since, the DR method imposes limitations on the homogeneity of the adsorbent, it may not be the most appropriate model for heterogeneous materials.[40] Therefore, Dubinin, Radushkevich, and Astakhov proposed a new equation (DA equation) which should be applicable to a wider range of heterogeneous microporous adsorbents. Since, SWNTs are heterogeneous adsorbents selecting DA model for this study was considered appropriate. The DA method is described as,

$$W = W_0 \exp\left[-\left(\frac{-RT \ln P/P_o}{E} \right)^n \right] \qquad (12)$$

where *n* is the exponent (typically 1 < *n* < 3), which reflects the width of the energy distribution and itself is related to the pore size distribution[41]. In the limiting cases with *n* = 2, the DA equation reduces to DR equation, i.e., the heterogeneous microporous structures become homogeneous. It has been shown that for strongly activated and heterogeneous carbons, the values of n are at the range of 1.5 < *n* < 2, whereas for molecular-sieve carbons the values of *n* are close to 3[42].

2.2.2 New Method

A new method to estimate micropore volume and external surface area, specific to SWNTs, was developed by Agnihotri *et al*., 2005. This method is a sub-set of the global methodology for representing *heterogeneity* of SWNTs for grand canonical

Monte Carlo (GCMC) simulations created by these authors. Following is a description of the same.

Modeling a heterogeneous bundle of SWNTs with an exact distribution and positional arrangement of individual SWNTs in the sample could be an extremely time consuming and complicated work. Therefore, theoretical modeling of heterogeneity could become sample specific; it may or may not be extended to the variety of samples that are now being synthesized worldwide. A practical approach for theoretical modeling of heterogeneity of SWNT bundles has been developed in 2005[21]. It integrates sample morphology, especially diameter distribution and sample purity, into GCMC simulation. GCMC calculations are carried out in three steps (Figure 2.7).

Step 1: A heterogeneous bundle (Figure 2.7 (a)) is deconvoluted into several homogenous bundles (Figure 2.7 (b)). The tube-diameter distribution for a given SWNT sample can be obtained from the radial breathing mode (RBM) region of the spectrum at a given excitation energy λ, e.g. $\omega_{\mathrm{RBM}} = 12.5 + 223.5/D\,(\mathrm{nm})$ for λ = 785 nm, where *D* is the tube diameter and ω_{RBM} is the corresponding RBM frequency in the 100-300 cm^{-1} region.

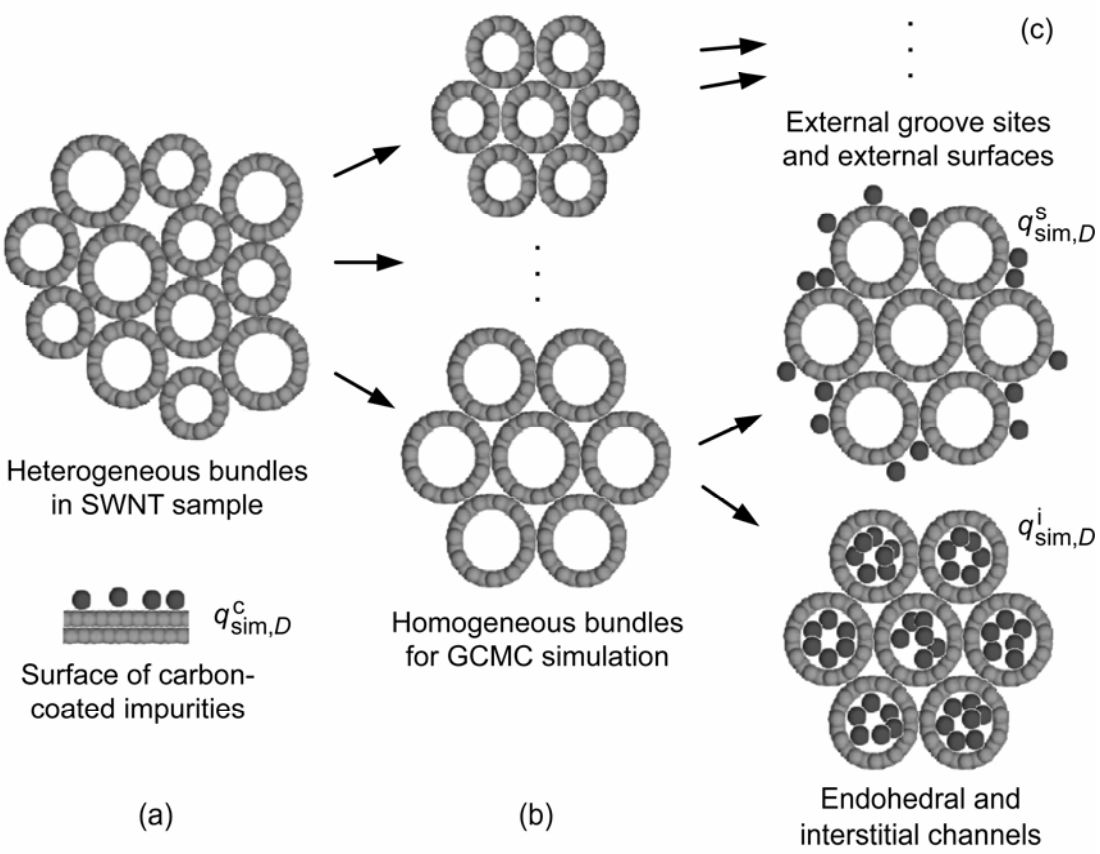

Figure 2.7. (a) Depiction of a typical heterogeneous SWNT bundle; the presence of impurities is approximated by an equivalent amount of planar nonporous carbon (q^{s}_{sim}). (b) Deconvolution of the heterogeneous bundle into several homogeneous bundles; the tube diameter, *D*, for each homogeneous bundle is determined from Raman scattering experiments. (c) GCMC simulation of adsorption on the external grooves and external surfaces (q^{s}_{sim}) and in the internal accessible volume (q^{i}_{sim}) of each homogeneous bundle. Total adsorption for the heterogeneous bundle is determined by weighted averaging of the individual contributions over the tube-diameter distribution obtained at each excitation energy λ.

Step 2: Each homogeneous bundle is further deconvoluted into two parts: the endohedral volume and the exohedral surface of the outermost SWNTs in the bundle (Figure 2.7 (c)). The former comprises adsorption inside the nanotubes and in the interstitial channels, whereas the latter represents adsorption in external groove sites and external surfaces, including the void space between the bundles. For each of these configurations, GCMC simulations of a small probe molecule are then carried out for comparison with experimental adsorption at same temperature and pressure conditions. For N_2 adsorption at 77 K, each nanotube can be approximated as a smooth structureless nanocylinder. The intertube distance for all simulation is kept fixed at 3.4 Å to mimic SWNTs adhering to each other via van der Waals forces forming bundles. Nitrogen is treated as a structureless spherical particle which interacts via dispersive forces only. The interaction between adsorbate molecules is modeled by a 12-6 Lennard-Jones (LJ) potential, $u_{ij} = 4\varepsilon_{ij}\left[(\sigma_{ij}/r)^{12} - (\sigma_{ij}/r)^{6}\right]$ (r is the intermolecular distance), as is the interaction between the carbon atoms of a nanotube and each adsorbate site. The well depths, ε_C/k_B and ε_{N2}/k_B (k_B is Boltzmann constant), used in calculations are 28.0 K and 100.4 K, respectively, and the collision diameters, σ_C and σ_{N2}, are 3.4 Å and 3.69 Å, respectively; the cross terms are obtained using standard Lorenz-Berthelot combination rules: $\varepsilon_{ij} = (\varepsilon_i \varepsilon_j)^{1/2}$ and $\sigma_{ij} = (\sigma_i + \sigma_j)/2$. The potential parameters for N_2 were obtained by fitting the simulated vapor-liquid coexistence curve to experimental data. Using these interaction parameters we have obtained very good agreement between the

simulated N_2 adsorption isotherm and experimental data for nonporous carbon, which indicates that these parameters are a good first approximation to the adsorbate-nanotube interaction potential at the temperature of interest. The carbonaceous impurities are modeled as stacked graphene layers, with platelet spacing of 3.4 Å, using Steele's 10-4-3 potential. The GCMC simulations are carried out using established procedures;[43-47] the reader is referred to previous work[21, 48-50] for further details.

Step 3: Once the endohedral and exohedral isotherms for each homogenous bundle have been calculated, they are weight-averaged according to the tube-diameter distribution obtained from the relative peak intensity at each RBM frequency. This provides theoretical isotherms, $q^{\mathrm{s}}_{\mathrm{sim}}$ and $q^{\mathrm{i}}_{\mathrm{sim}}$, incorporated with sample-specific heterogeneity:

$$\left\{q^{\mathrm{s}}_{\mathrm{sim}}, q^{\mathrm{i}}_{\mathrm{sim}}\right\} = \frac{1}{n_\lambda}\sum_{\lambda}\sum_{D} w_{\lambda,D}\left\{q^{\mathrm{s}}_{\mathrm{sim},D}, q^{\mathrm{i}}_{\mathrm{sim},D}\right\},\ \sum_{D} w_{\lambda,D} = 1. \qquad (13)$$

Here, $q^{\mathrm{s}}_{\mathrm{sim},D}(P/P_{\mathrm{o}})$ and $q^{\mathrm{i}}_{\mathrm{sim},D}(P/P_{\mathrm{o}})$ are the adsorption isotherms for the external surface (s) and internal volume (i) of an homogeneous bundle of tube diameter *D*, expressed as a function of relative pressure P/P_{o}; Σ_λ denotes summation over the n_λ excitation energies probed in the Raman scattering experiments; $w_{\lambda,D}$ is the tube-diameter distribution obtained at a particular excitation energy λ, which can be estimated from the relative ratio of peak heights at the corresponding ω_{RBM} in the Raman spectrum.

The total adsorption isotherm for the sample, $q_{sim}(P/P_o)$, is then expressed as

$$q_{\mathrm{sim}}(P/P_{\mathrm{o}}) = \underbrace{(1-\eta)q^{\mathrm{i}}_{\mathrm{sim}}(P/P_{\mathrm{o}})}_{\text{(endohedral)}} + \underbrace{S_{\mathrm{p}}q^{\mathrm{s}}_{\mathrm{sim}}(P/P_{\mathrm{o}})}_{\text{(exohedral)}} + \underbrace{S_{\mathrm{c}}\eta q^{\mathrm{c}}_{\mathrm{sim}}(P/P_{\mathrm{o}})}_{\text{(impurities)}} \qquad (14)$$

where η is the weight-fraction of impurities in the sample, S_{p} is the external surface area of SWNTs in the sample (m^2/g); S_{c} is the surface area of impurities (m^2/g), and $q^{\mathrm{c}}_{\mathrm{sim}}(P/P_{\mathrm{o}})$ is the adsorption isotherm on nonporous carbon, which is assumed to be representative of the adsorptive contribution from carbon-coated impurities. In a related work,[49] it has been shown that most impurities present in SWNT samples can be modeled as the planar surface of a nonporous carbon, and S_{c} can be calculated by least-square fitting of Eq. 14 to the experimental data. Note that the first term on the r.h.s. of Eq. 14 is the total endohedral adsorption in the nanotube bundles; the other two terms account for adsorption outside of the internal accessible porous volume of the nanotubes, i.e. adsorption on the *external surface* and on *impurities*.

2.2.2.1 Micropore Volume and External Surface Area

It is to be noticed that in their calculations, endohedral adsorption is expressed as amount adsorbed per unit weight (mol/g or cm^3[STP]/g) of bundle, whereas exohedral adsorption is calculated as amount adsorbed per unit external surface area of the bundle (mol/m^2 or cm^3[STP]/m^2); if the latter value is multiplied by the specific external surface area, S_p (m^2/g), the adsorption isotherm for the external surface

becomes expressed per unit weight also. Thus, the calculation of the total adsorptive contribution from the external surface of the bundle requires the estimation of S_p.

These authors also developed a method of estimating the external surface areas (i.e., S_p in Eq. 14). It was determined by plotting the total experimental adsorption capacity of the samples (cm^3[STP]/g of sample) against the simulated amount adsorbed on the external surface of the bundle (cm^3[STP]/m^2 of nanotubes), at same P/P_o (Figure 2.8). The plots are interpreted to comprise of two regions: the first region shows a steep rise and the second region that nearly follows a straight line. The first region of the curve indicates that the experimental adsorption capacity surpassed the simulated values, which means that internal adsorption in the sample was much higher than external adsorption.

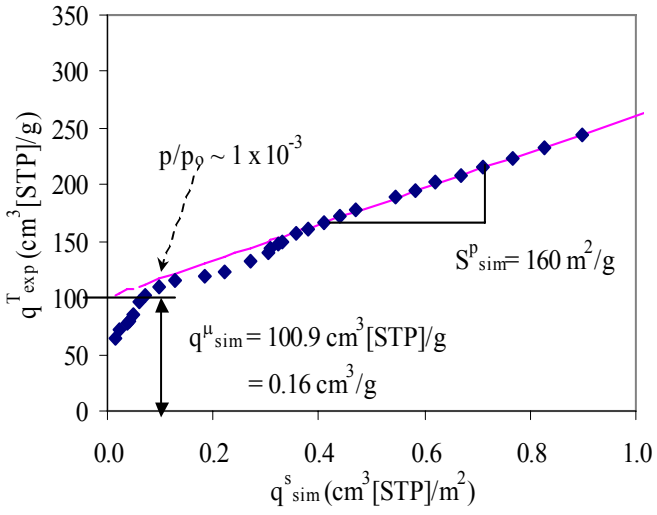

Figure 2.8. Representative figure for estimating Micropore Volume and External Surface Area for impurity free (S_c = 0) sample.

The second region of the curve implies that the experimental adsorption capacity was linearly proportional to the simulated external adsorption capacity or, in other words, majority of adsorption in the sample occurred on the external surface of the bundles. The slope of the second region of the curve, thus, represents the total external surface area of nanotubes in the sample. Additionally, the intercept of the straight line through the linear part of the curve provides the micropore volume of the sample because the amount adsorbed at zero surface-loading is adsorbed entirely inside the pores. Therefore, the intercept should be the micropore volume of the sample. In summary, plotting the experimental adsorption isotherm versus the simulated exohedral adsorption isotherm yields a curve, whose slope of the linear asymptote at high loading gives the value of S_p.

Chapter 3

RESULTS AND DISCUSSION

3.1 Sample Morphology

3.1.1 Raman Spectroscopy

Since Raman scattering by single excitation energy may not be sufficient to explore all of the SWNT diameters. In this study, multiple excitation energies of Raman scattering, which are at $\lambda = 532$ nm, $\lambda = 633$ nm, and $\lambda = 785$ nm, were used on all of the four samples listed in Table 3.1.

Including 3 excitation energies of Raman scattering on SWNT samples, Figure 3.1 depicts the RBM region of the Raman spectra for samples EA95 and CVD95. It is shown that CVD95 sample is more heterogeneous and has a higher concentration of smaller carbon nanotubes compared to EA95 sample. Each spectrum shows the presence of multiple diameters specific to the laser energy used in the Raman scattering experiments. Similar spectra were obtained for the other two samples, CS70 and BU90. The discrete values of *D* calculated for all samples in Table 3.1.

Table 3.1. RBM frequencies for SWNTs samples tested

Sample	Diameter (nm)*		
	$\lambda = 532$ nm	$\lambda = 633$ nm	$\lambda = 785$ nm
EA95	1.37, 1.54	1.25, 1.30, 1.43	1.15, 1.40, 1.52
CVD95	0.92, 1.56	0.80, 0.84, 0.92, 1.09, 1.23	0.90, 1.02, 1.07, 1.11, 1.18
CS70	1.46, 1.60	1.25, 1.41	/
BU90	0.85, 0.95, 1.17, 1.32, 1.67	0.92, 1.11, 1.22, 1.34	/

* calculated from Eq. 1.

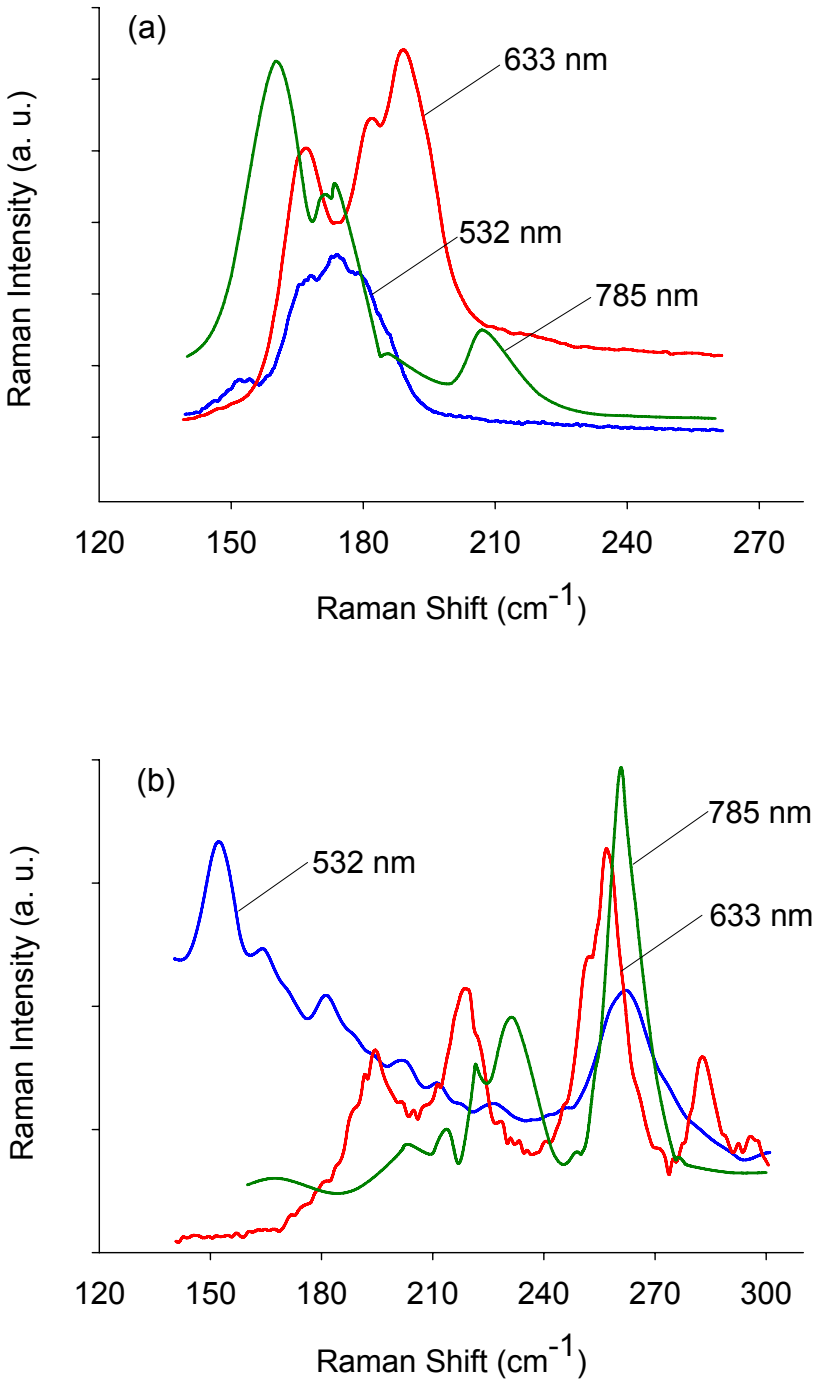

Figure 3.1. RBM region of Raman spectra for SWMT samples (a) EA95 and (b) CVD95. Similar spectra were collected for all samples.

3.1.2 TGA

SWNT samples were analyzed for purity by TGA (Perkin-Elmer TGA Pyris 1). In the new characterization method, sample purity needs to be estimated from the purity value provided by the manufacturer. Because of the exceptionally high level of purity for sample EA95 and relatively lower level of purity for sample CS70, the TGA results of samples EA95 and CS70 were selected to be reported.

For statistical purposes three experiments per sample were performed in this study. For sample EA95, no residue was observed in the sample pan, which showed the absence of catalytic material. Alternatively, approximately 10 wt% of catalyst, i.e., Ni, was observed for sample CS70, after correcting the residual mass for catalyst oxidation. The purity of sample could be accessed by plotting the weight loss versus the time curve as rate of weight loss (d*wt*/d*t*) versus time curve (Figure 3.2). Due to the fact that different structure types of carbon oxidize at varying rates and onset temperature, the carbon sample that consists of a mixture of different types of carbons will give multiple peaks in the d*wt*/d*t* versus *t* curve.

It is shown that for sample EA95 the d*wt*/d*t* versus *t* curve exhibited only one peak (Figure 3.2 (a)), which shows the presence of only one type of carbon; whereas for sample CS70 the d*wt*/d*t* versus *t* curve exhibited four peaks (Figure 3.2 (b)). For the

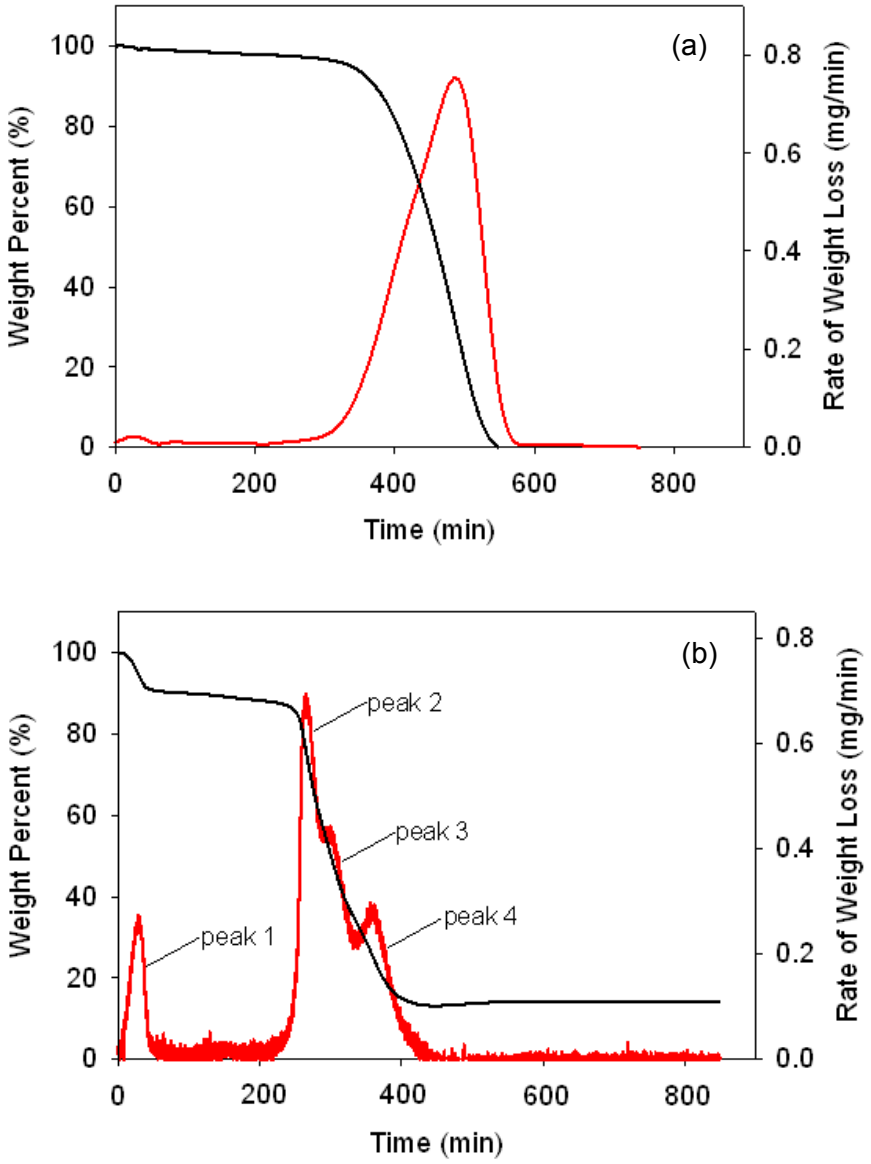

Figure 3.2. Estimate of sample purity by TGA. (a) EA95 sample from MER Corp.; (b) CS70 sample from Carbon Solution.

peak 1, which appears at 100^{o}C, it shows the water decomposition. For the peak 2 and 3, which appear at 560^{o}C and 600^{o}C, they denoted that SWNTs were burned at that range of temperature. The last peak (peak 4) stands for graphite. The area under the curves of peak 2 and 3 corresponded to about 69.1% of sample mass, which is pretty close to the given purity of 70 wt% of SWNT. Similarly, the area under the curve in Figure 3.2 (a) corresponded to 95-98% of sample mass, which is also quite close to the given 95 wt% purity. It can be concluded that EA95 sample contained almost pure SWNTs with composition similar to that reported by the manufacturer. The purity of sample CS70 was also confirmed to approximately 70 wt% by TGA analysis.

3.1.3 XPS

XPS experiments were performed to further confirm the TGA results on all SWNT samples. With the lowest purity of all tested samples, CS70 was shown containing about 10% catalyst by TGA experiment. However, XPS survey scan does not show any metal peak (Figure 3.3). It is known that XPS only explores few 10s of Å beneath the top layer of the material. While catalytic impurities are covered with at least few atom thick layer of carbon. Therefore, catalyst contribution is included in the C peak and it is reasonable to use planar carbon as impurities of samples in this study. Figure 3.3 is collected spectra about the estimates of atomic and weight concentrations of the aim elements, carbon and oxygen (96.2% and 3.8% respectively).

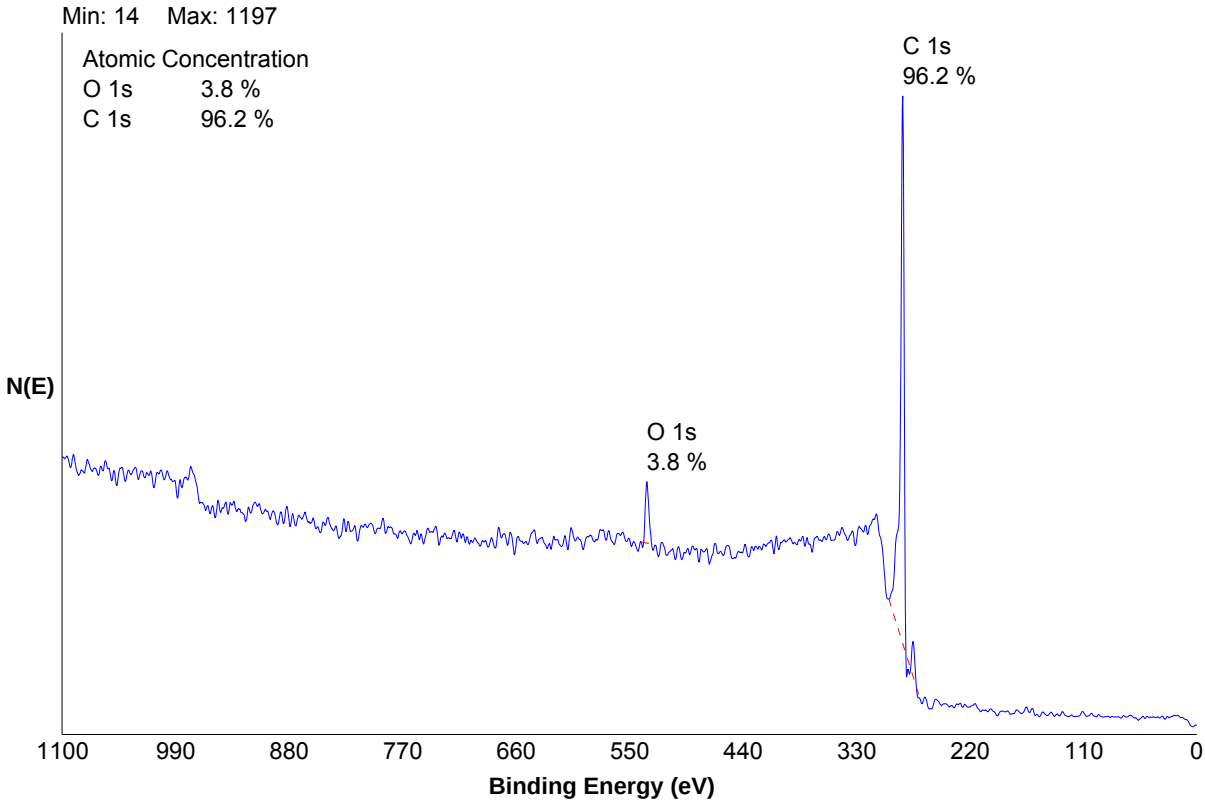

Figure 3.3. Survey scan of XPS experiment for SWNT sample CS70.

3.2 Pore volume and surface area of SWNTs

3.2.1 t-plot Method

The t-plot method was applied to four SWNT samples, EA95, CVD95, CS70, and BU90, which has > 95 wt%, > 95 wt%, 70 wt%, and 90 wt% purity, provided by the manufacturers. The micropore volume and external surface area of the samples were specific to the three equations commonly used in calculating statistical thickness, *t*. Furthermore, the t-plot did not always follow a straight line in the suggested pressure range of $0.05 < P/P_o < 0.35$. Representative values are provided in Table 3.2, whereas Figure 3.4 shows t-plot procedure to calculate the micropore volume and external surface area of SWNT samples.

Table 3.2. Micropore volume (cm^3/g) and external surface area (m^2/g) of SWNTs determined from three equations commonly used for calculating *t* in the t-plot.

Sample	Micropore Volume (cm^3/g)				External Surface Area (m^2/g)			
	Eq.2	Eq.3	Eq.4	**Avg.**	Eq.2	Eq.3	Eq.4	**Avg.**
EA95	0.155	0.151	0.101	**0.136±0.030**	303	313	361	**326±31**
CVD95	0.054	0.047	0	**0.034±0.029**	593	614	706	**638±60**
CS70	0.151	0.143	0.030	**0.108±0.068**	681	705	812	**733±70**
BU90	0.018	0.010	0	**0.009±0.009**	600	623	713	**645±60**

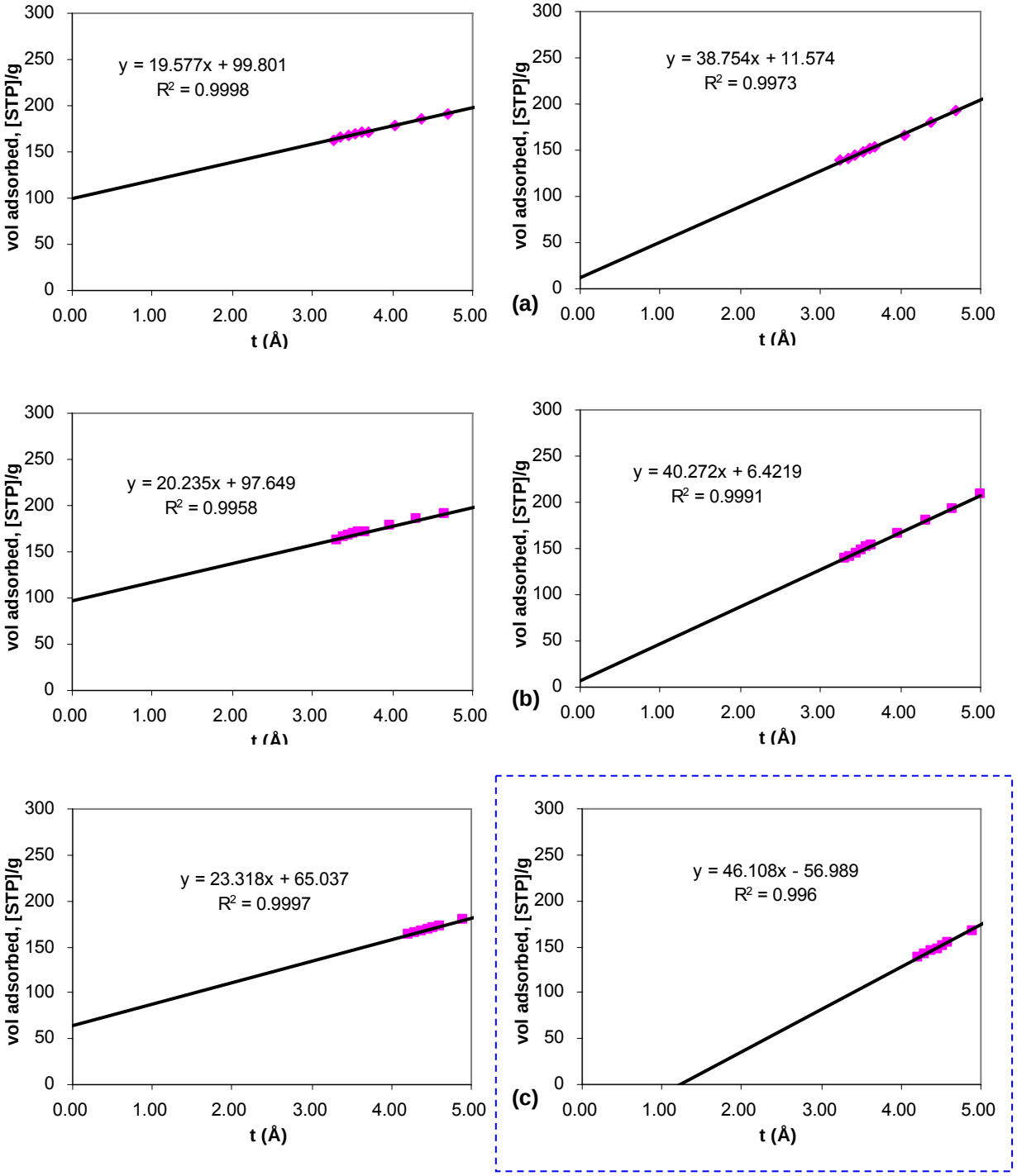

Figure 3.4. t-plot for SWNT samples EA95 (left) and BU90 (right) where t is estimated by (a) de Boer equation (Eq. 2), (b) Carbon Black equation (Eq. 3), and (c) Halsey equation (Eq. 4). The figure highlighted in blue dashed line shows an unexpected result (negative micropore volume) for BU90 sample.

For the t-plot method, by plotting the adsorption capacity versus the statistical thickness (Figure 3.4), Eq. 6 and 7 were then used to calculate the micropore volume and external surface area, respectively (Table 3.2). In the recommended relative pressure range of $0.05 < P/P_o < 0.35$, the t-plots for EA95 (Figure 3.4 left) sample yield straight lines as using three common equations; whereas the t-plot for BU90 (Figure 3.4 right highlighted in blue) sample by using Halsey equation gives negative intercept. Accordingly the micropore volume for this sample is assumed as zero (Table 3.2). Similar results can be obtained for other two samples CS70 and CVD95 (Figure 3.5).

The results in Table 3.2 varied in a wide range in both the micropore volume and external surface area values by using different equations in t-plot method. Take the results of sample CS70 for example, the average micropore volume is 0.108 cm^3/g, whereas the results obtained from Eq.2, Eq.3, and Eq.4 are in the range of 0.030 to 0.151 cm^3/g. Similarly, the average external surface area of CS70 sample is 733 m^2/g, whereas the results obtained from Eq.2, Eq.3, and Eq.4 are in the range of 681 to 812 m^2/g. Therefore the t-plot method could not give consistent results for SWNT samples by switching equations in the calculation. These results demonstrate the t-plot method used for physical characterization of common adsorbents may not be applicable to carbon nanotubes.

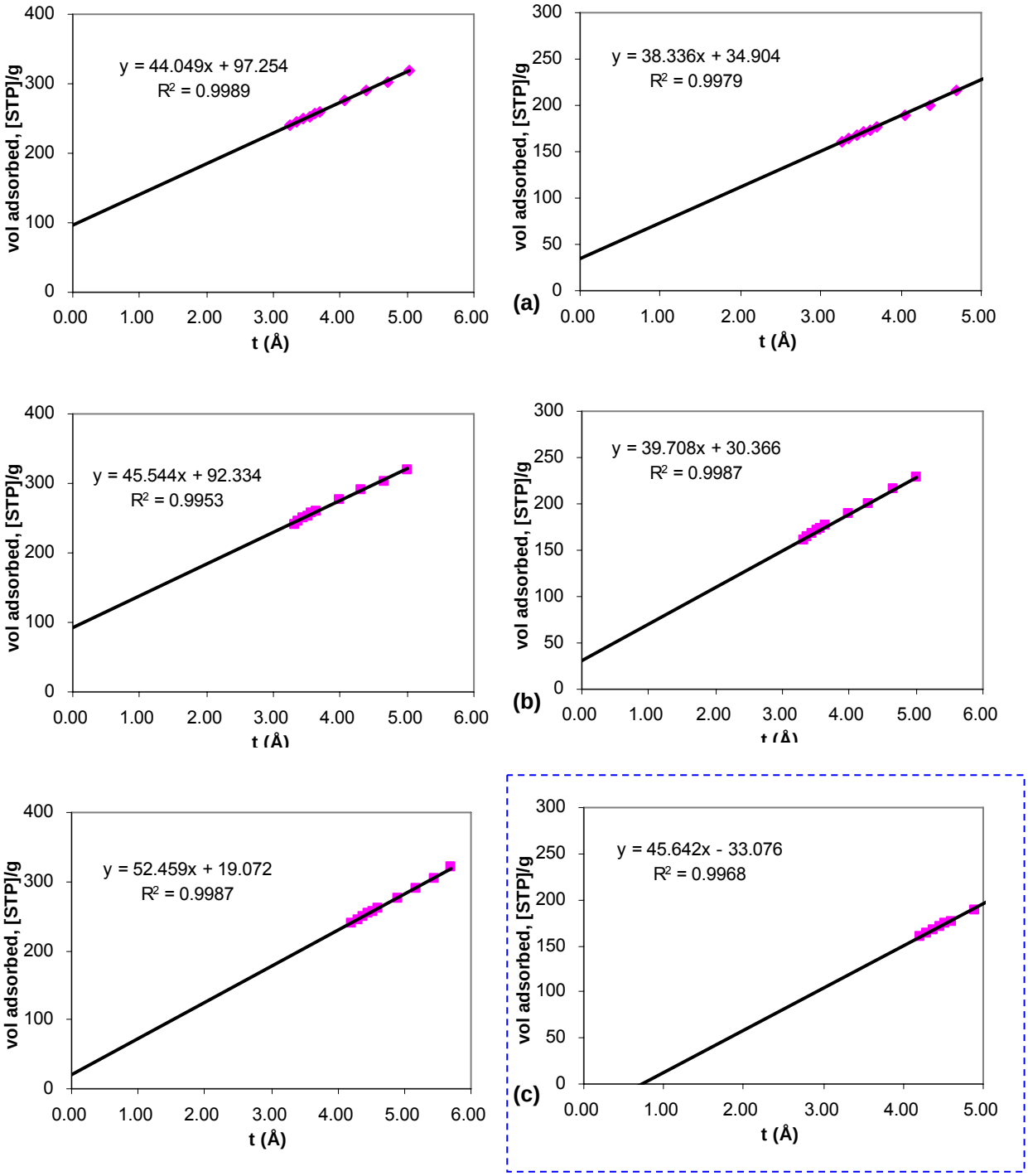

Figure 3.5. t-plot for SWNT samples CS70 (left) and CVD95 (right) where t is estimated by (a) de Boer equation (Eq. 2), (b) Carbon Black equation (Eq. 3), and (c) Halsey equation (Eq. 4). The figure highlighted in blue dashed line shows an unexpected result (negative micropore volume) for CVD95 sample.

3.2.2 DR/DA Method

As a homogeneous micropore structure analysis method, DR method was applied by using Quantachrome Autosorb 1 software. On the other hand, DA method, which was developed for heterogeneous micropore structure, was also applied by using Quantachrome Autosorb 1. For each of the tested SWNT samples, the analysis by either DR or DA method was performed at the same relative pressure range. The representative values are provided in Table 3.3.

Table 3.3. Micropore volume (cm^3/g) and micropore surface area (m^2/g) of SWNTs determined from DR/A method.

Sample	DR Method			DA Method			
	E_0 (kJ/mol)	μV* (cm^3/g)	μSA** (m^2/g)	E (kJ/mol)	n	μV* (cm^3/g)	μSA** (m^2/g)
EA95	22.1	0.24	675	7.41	1.2	0.32	890
CVD95	14.7	0.26	728	4.87	1.5	0.34	945
CS70	17.2	0.375	1050	6.34	1.7	0.42	1170
BU90	11.6	0.304	853	3.97	1.7	0.39	1110

*μV represents micropore volume; **μSA represents micropore surface area.

The results show that both micropore volume and micropore surface area values of SWNT samples varied greatly different for DR and DA methods. Take the results of sample EA95 for example, the micropore volume obtained from DR method is 0.24 cm^3/g, whereas the result obtained from DA method is 0.32 cm^3/g. It gives an approximate error of 25%. The micropore surface area of CS70 obtained from DR method is 675 m^2/g, while the result obtained from DA method is 890 m^2/g. The surface area results also give an approximate error of 24%. From Table 3.3, the highest micropore volume and micropore surface area values are from CS70 sample, of which are 0.42 cm^3/g and 1170 m^2/g, respectively. Compared to the previous work[12], reported as 0.15 cm^3/g and 314 m^2/g, these values in Table 3.3 are too high to be reasonable.

3.2.3 New Method and Proposed Modification

The total adsorption isotherm for the sample, $q_{sim}(P/P_o)$, is expressed as

$$q_{\mathrm{sim}}(P/P_{\mathrm{o}}) = \underbrace{(1-\eta)q^{\mathrm{i}}_{\mathrm{sim}}(P/P_{\mathrm{o}})}_{\text{(endohedral)}} + \underbrace{S_{\mathrm{p}}q^{\mathrm{s}}_{\mathrm{sim}}(P/P_{\mathrm{o}})}_{\text{(exohedral)}} + \underbrace{S_{\mathrm{c}}\eta q^{\mathrm{c}}_{\mathrm{sim}}(P/P_{\mathrm{o}})}_{\text{(impurities)}} \qquad (14)$$

The adsorption isotherm on external surface (q^s_{sim}) of the SWNT bundles, and the isotherm on non-porous carbon (q^c_{sim}) are taken from the previous GCMC simulation work[21]. Total 35 adsorption data points are presented in Table 3.4 and then plotted in Figure 3.6.

Table 3.4. GCMC simulated data of N_2 adsorption isotherm (77 K) on external surface of SNWT bundles (q^s_{sim}) and on nonporous carbon (q^c_{sim}).

P/P_o ([STP])	q^s_{sim} (cm^3 [STP]/cm^2)	q^c_{sim} (cm^3 [STP]/cm^2)
1.00E-06	0.002	2.0E-04
3.00E-06	0.006	5.0E-04
5.00E-06	0.010	8.0E-04
1.38E-05	0.023	2.2E-03
3.50E-05	0.037	5.5E-03
5.00E-05	0.041	9.8E-03
1.00E-04	0.047	4.6E-02
3.00E-04	0.055	1.2E-01
5.00E-04	0.060	1.6E-01
1.00E-03	0.069	1.9E-01
2.00E-03	0.089	2.1E-01
3.00E-03	0.113	2.1E-01
5.00E-03	0.162	2.2E-01
7.50E-03	0.201	2.2E-01
1.00E-02	0.221	2.3E-01
2.00E-02	0.254	2.4E-01
4.00E-02	0.276	2.5E-01
6.00E-02	0.286	2.5E-01
8.50E-02	0.295	2.7E-01
1.10E-01	0.303	2.8E-01
1.50E-01	0.316	3.1E-01
1.80E-01	0.326	3.4E-01
2.00E-01	0.335	3.6E-01
2.60E-01	0.364	4.1E-01
3.00E-01	0.393	4.3E-01
3.50E-01	0.424	4.6E-01
4.50E-01	0.503	5.1E-01
5.00E-01	0.522	5.4E-01
5.50E-01	0.552	5.7E-01
6.00E-01	0.582	6.2E-01
6.50E-01	0.616	6.6E-01
7.00E-01	0.658	7.1E-01
7.30E-01	0.711	7.4E-01
7.50E-01	0.726	7.6E-01
7.80E-01	0.784	7.9E-01

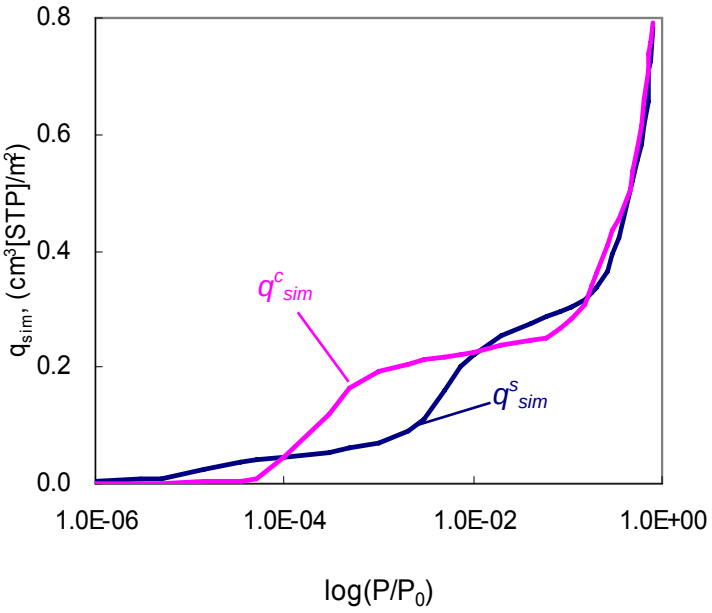

Figure 3.6. Adsorption isotherms on external surface of SWNT bundles (pink) and on nonporous carbon (blue) by GCMC simulation.

The previous method (Agnihotri et al., 2005) was based on plotting the total experimental adsorption capacity of the samples (Y axis) against the simulated amount adsorbed on the external surface of the bundle (X axis, Figure 2.8). This method corresponded to a special case of $\eta = 0$, or in other words, it corresponded to samples virtually free of impurities. However, for partially purified samples with some impurities ($\eta > 0$), this relatively straight-forward method is not applicable. Therefore, these authors suggested fitting Eq. 14 to the experimental data by least-square fitting, i.e., q_{sim} (P/P_o) = q_{exp} (P/P_o). The fitting is performed by a computer-code that yields surface area of bundles and impurities (i.e., S_p and S_c) and pore volumes as fitting parameters. Although, this method provided a good estimate of these parameters

(Agnihotri et al., 2006), it is not readily useable simply due to the need for sophisticated computational tools including MATLAB^{TM} and its working knowledge. Therefore, we have developed a new method that uses the same simulation data but interprets in a way that the straight-line method is applicable to impure samples. This is presented next.

3.2.3.1 New Definition of t

To make the straight-line method applicable to impure samples, we propose a new definition of statistical thickness, *t,* which is specific to SWNTs. We noticed that in the early works of Agnihotri *et al*., the use of q_{sim} was similar to that of the statistical thickness; however, the thickness is just happened to be expressed in different units. For example, in the t-plot method the statistical thickness is defined as the thickness of the adsorbate layer and is expressed in nm. On the other hand, the new method also plots the same information but on the basis of the simulated adsorption isotherm, q_{sim}, which is defined as the amount of the adsorbate layer and is expressed in the unit of cm^3 [STP]/m^2. We observed that the new-method was complimentary to the t-plot method. Furthermore, Agnihotri *et al*.,[49] showed that impurities in SWNT samples can be modeled as planar carbon. The N_2 adsorption capacity of planar carbons (Table 3.4) was calculated by using the GCMC technique mentioned above. We developed a new equation (Eq. 15) upon incorporating adsorption on the planar

carbon to represent impurities with that on the external surface of the SWNTs bundles. This equation is represented as true statistical thickness, *t*.

$$t = f\left(q^{s}_{sim}\right)_{SWNTs} + \left(1-f\right)\left(q^{c}_{sim}\right)_{impurities} \quad (15)$$

Here, we introduce a new parameter *f* which is a unitless floating parameter that can be determined by trial-and-error in a way that minimizes the overshoot.

Figure 3.7 shows plot of experimental isotherm data (Y axis) and *t* (X axis) as calculated by our proposed Eq. 15 for several values of *f*. The plot is more or less a straight line. This supports our hypothesis that an interpretation of the simulated data as simply a new form of the statistical thickness is correct. SWNT sample CS70, which is 70 wt% of SWNT, was selected to be the impure sample for further study. To find the correct value of *f*, an extreme case of *f* = 1 was first used to start the analysis. This resulted in an obvious overshoot (highlighted in blue dashed circle) of the curve same as that in Figure 3.7 (a). The overshoot suggests that *f* is over-estimated. Then a smaller value of *f* = 0.8 was selected and the curve seems to be flattened (Figure 3.7 (b)). In this case, the difference between experimental values and fitted line seems being reduced. Then the value of *f* was further reduced to 0.7 at which the fitted line superimposed the experimental data with no observable differences (Figure 3.7 (c)). This trend seems to be complying with our hypothesis which forms the basis for Eq. 15. Once the value of *f* was reduced to 0.7, the further reduction of *f* value resulted in no obvious changes between the data and the fitted line (Figure 3.7 (d)).

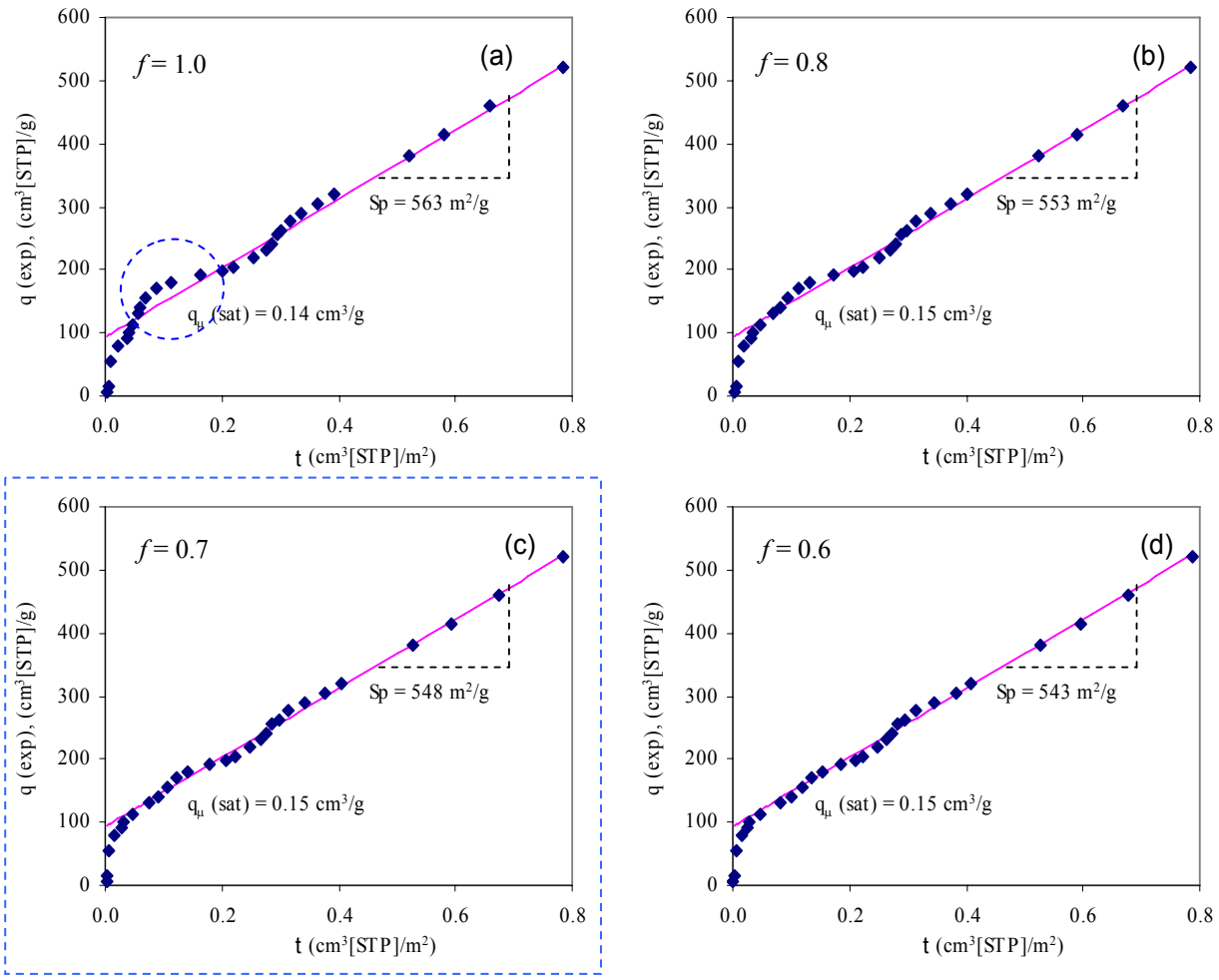

Figure 3.7. Total experimental adsorption capacity versus simulated surface adsorption capacity for impure sample CS70 with *f* = (a) 1.0 (b) 0.8 (c) 0.7 and (d) 0.6. The intercept and slope of the straight line represents micropore volume and external surface area of the sample.

It was noticed that the surface area decreased slightly with decreasing values of *f*; whereas the micropore volume slightly increased. It was also noticed that the *f* value at which the overshoot is nullified (Figure 3.7 (c)) was corresponded to the purity of the sample (i.e., *f* = 0.7 stands for 70 wt% pure of SWNT sample). The similar results could be obtained for other SWNT sample tested in this study. Therefore, it is reasonable to conclude that this new method can be applied to a variety of SWNT samples with varying degrees of purity.

3.2.3.2 Application of New *t* to Various Samples

Apply the new statistical thickness, *t*, to various samples. The impurity of SWNTs was incorporated into the adsorption isotherms in this study. The modified method[21] plotted the adsorption capacity versus the new statistical thickness (Eq. 15), *t*, which was calculated by simulating the amount of N_2 adsorbed (cm^3 [STP]/m^2) on the external surface of the SWNT bundles. The micropore volume and external surface area of SWNT samples EA95, CVD95, CS70 and BU90 were determined (Figure 3.8). The plot could be interpreted to comprise of two regions: the first region shows a steep rise and the second region that nearly follows a straight line. The first region of the curve implies that the internal adsorption was much higher than that on its external surface; whereas the second region indicates that most of the adsorption in this pressure range occurred on the external surface of the SWNT bundles.

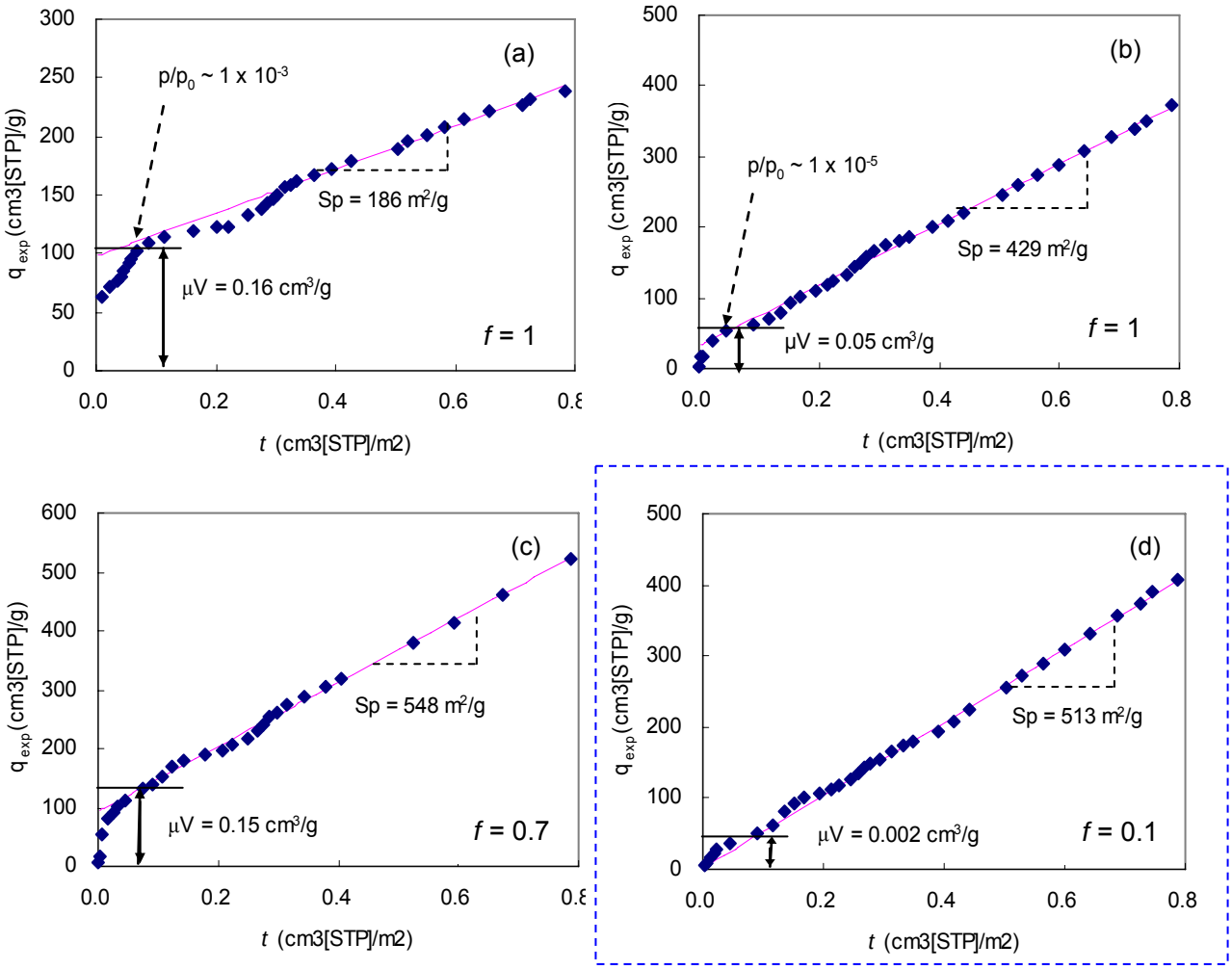

Figure 3.8. Total experimental adsorption capacity versus surface adsorption capacity for SWNT samples (a) EA95, (b) CVD95, (c) CS70, and (d) BU90. The intercept and slope of the straight line represent micropore volume and external surface area of SWNTs of the sample.

The intercept and slope of the straight line on the second region of curve represent the micropore volume and total external surface area of CNTs in the sample. The data fitting has been accomplished when the micropores of CNTs are filled, which indicated that the intercept of the fitted straight line is not a function of the relative pressure, P/P_0. At the critical point where the two regions of curve cross, the relative pressure indicates the maximum pressure above which the micropore of CNTs is filled. The plots show that the micropore of sample CVD95 is filled at pressure ($P/P_o \sim 10^{-5}$) much lower than that for sample EA95 ($P/P_o \sim 10^{-3}$). This can further confirm the tube diameter distribution results determined by Raman spectroscopy, which indicates that the CVD95 sample has smaller sized tubes than those of EA95 sample.

Table 3.5. Micropore volume (cm^3/g) and external surface area (m^2/g) of SWNTs determined from modified new method and t-plot method.

Sample	*f*	Micropore Volume (cm^3/g)			External Surface Area (m^2/g)		
		New method	Agnihotri, 2005	t-plot method	New method	Agnihotri, 2005	t-plot method
EA95	1.0	0.16	0.16	0.15	186	155	313
CVD95	1.0	0.05	0.05	0.04	429	541	614
CS70	0.7	0.15	0.15	0.14	548	656	705
BU90	0.1	0.002	0.02	0.01	513	588	623

* t-plot method results obtained by using Carbon Black equation.

As shown in Figure 3.8 (a), it should be noticed that the certain data points were above the fitted line when this straight line was extrapolated to the entire data in this plot. This means that the total adsorption on this sample was more than the predicted adsorption on the external surface of the SWNT bundles. Most likely certain amount of impurities in the sample has contribution to adsorption, which made it necessary to incorporate the impurity into the adsorption isotherms. The results showed in Figure 3.8 were summarized in Table 3.5, of which the results obtained from t-plot method by using Carbon Black equation are also included. It showed that the external surface area of sample CVD95 (429 m^2/g), sample CS70 (548 m^2/g), and sample BU90 (513 m^2/g) are all higher than that of sample EA95 (186 m^2/g), which indicates that EA95 sample has thicker SWNT bundles compared to other three samples.

3.2.3.3 Discussion on *f* versus Purity

It should be noticed that the intercept of the fitted line (Figure 3.8 (d)) is below zero. It indicates that the micropore volume of BU90 sample is less than zero, which is unreasonable. Incorporating impurity into the adsorption isotherms, 90% purity supposed to be used in the analysis of BU90 sample. However, compared to the 90% purity provided by manufacturer, only 10% purity was obtained from the adjusting of parameter *f*. Thus the adsorption on the pure SWNT bundles is overestimated. To confirm the 10% purity of BU90 sample, TGA and TEM experiments were performed.

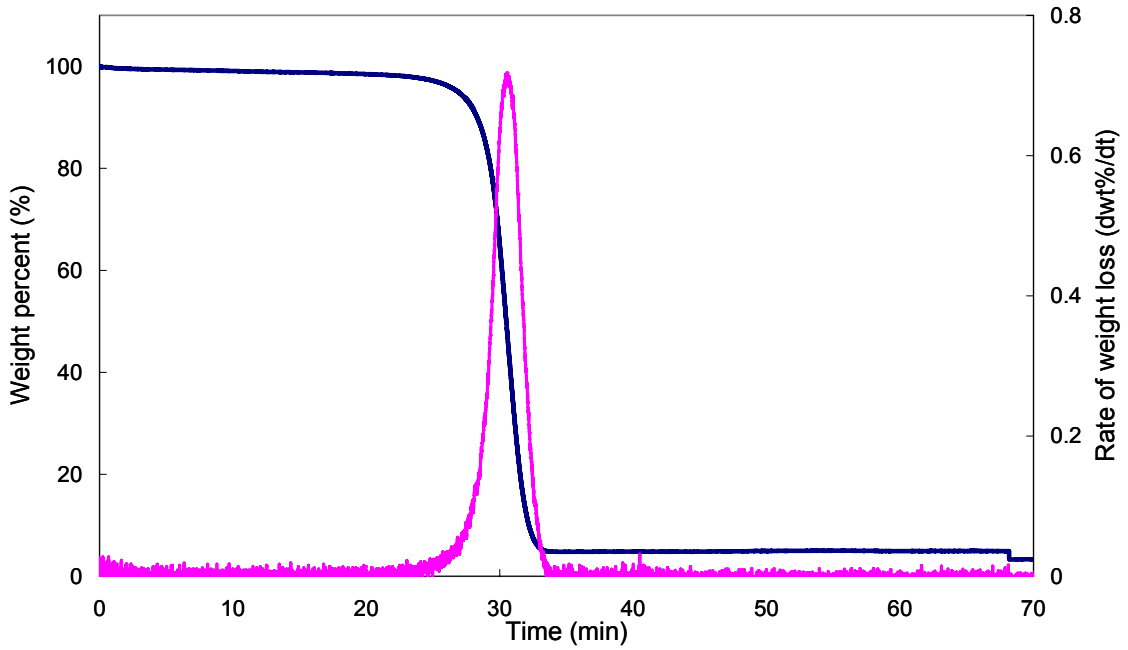

Figure 3.9. Estimate the sample purity of BU90 (Bucky USA) by TGA.

The purity of sample could be accessed by plotting the weight loss versus the time curve as rate of weight loss (d*wt*/d*t*) versus time curve (Figure 3.9). Due to the fact that different structure types of carbon oxidize at varying rates and onset temperature, the carbon sample that consists of a mixture of different types of carbons will give multiple peaks in the d*wt*/d*t* versus *t* curve. It is shown that for sample BU90 the d*wt*/d*t* versus *t* curve exhibited only one peak, which shows the presence of only one type of carbon. The weight loss peak, denoting the material burned at temperature of 640 ^{o}C, stands for graphite[51, 52]. Thus, the purity of SWNT of BU90 sample should be very low (less than 10%), which confirmed the *f* value determined from the new method.

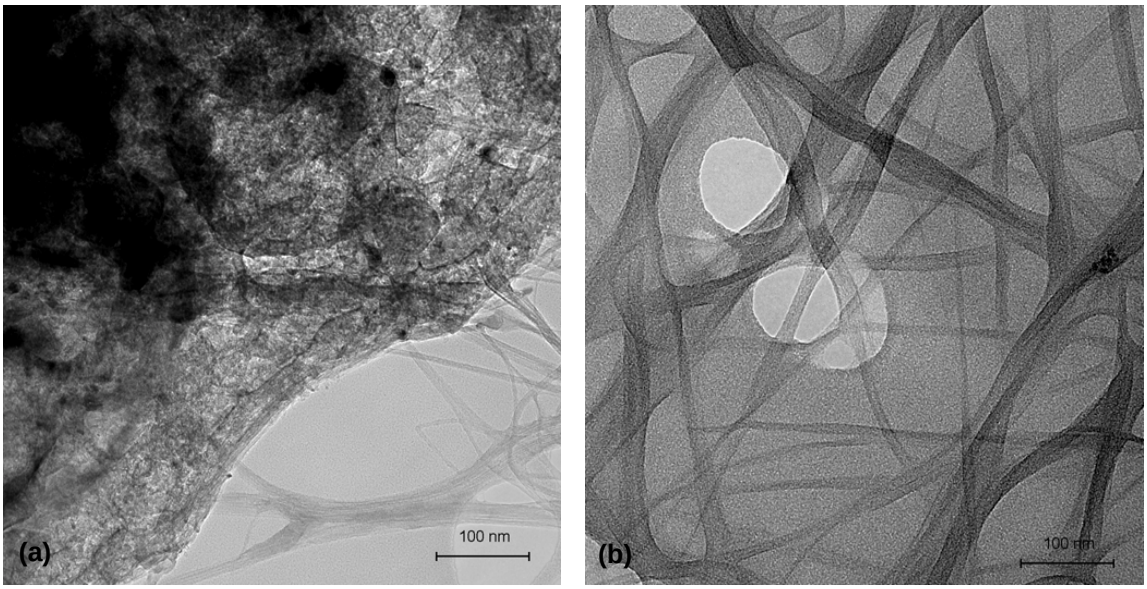

Figure 3.10. TEM images of (a) BU90 sample and (b) EA95 sample.

Figure 3.10 show the Transmission electron micrographs (TEM), taken from ORNL, of SWNT samples (a) BU90 and (b) EA95 with the same scale bar of 100 nm. Compared to the image (Figure 3.10 (b)) of very pure SWNT sample, EA95, the TEM image (Figure 3.10 (a)) of sample BU90 shows much less SWNT bundles, with smaller diameters. It is also confirmed our previous conclusion that the EA95 sample has thicker diameter of the SWNT bundles.

Chapter 4

CONCLUSIONS AND FUTURE RESEARCH

4.1 Conclusions

This study explored the morphology and adsorption properties of four commercially available SWNT samples, EA95, CVD95, CS70, and BU90. Two commonly used methods (t-plot method and DR/A method) and one relatively new developed method (Agnihotri, 2005 straight line method) were applied to all of the four samples to estimate the microporosity and surface area of SWNTs. The morphology of SWNT samples was determined by Quantachrome, TGA, Raman spectroscopy, and XPS. The EA95 and CVD95 samples have high purity with no apparent catalyst or amorphous carbon, which is consistent with the purity degrees of the samples provided by the manufacturer.

Compared to the two commonly used methods, t-plot method and DR/A method, the new developed straight line method is a microporosity and surface area estimation method, which is specific to SWNT samples. In traditional t-plot method and DR/A method, micropore volume and surface area of SWNTs can be determined by plotting the adsorption capacity versus statistical thickness, t, of adsorbed layer, of which the intercept and slope of the fitted line give the micropore volume and surface area of

sample, respectively. As one of the most commonly used method, t-plot method could be applied by several equations, such as de Boer equation (Eq. 2), Carbon Black equation (Eq. 3), and Halsey equation (Eq. 4) used in this study. The estimated micropore volume and surface area is always specific to the model and equation used in the analysis and also specific to the segment of adsorption isotherm, which is fitted to the model. SWNTs are relatively new adsorbents so that the applicability of these methods to carbon nanotuebs needs to be evaluated.

Agnihotri, *et al*. developed a new method that combined GCMC simulation, Raman spectroscopy, and standard N_2 adsorption (77K) to estimate the microporosity and surface area of SWNT samples. Similar to the t-plot method, this approach plots the total experimental adsorption capacity vs. simulated external adsorption capacity from SWNT bundles, which yields a more or less straight line for adsorption at $P/P_o \geq 10^{-3}$. Similarly, the intercept and slope of the line represent the micropore volume and the external surface area of the bundles, respectively. In this study, impurity was incorporated into adsorption by modeling it as planar carbon and adding it to the adsorption contributions. The main advantage of the new method is that it is applicable and specific to SWNTs samples. Furthermore, unlike the traditional methods, the new method includes the entire experimental adsorption isotherm ($10^{-6} < P/P_o < 0.99$) in analysis, thus minimizing any experimental errors related to selecting an appropriate segment of an experimental isotherm to fit the data.

4.2 Recommendation of Future Study

The future of carbon nanotubes in the environmental field applications is very promising. As a very fundamental research about the adsorption property of SWNT samples, this study performed a new technique to characterize nanotubes before they could be fully used in the practical area.

To further validate the applicability of the new method to carbon nanotubes in estimating micropore volume and external surface area, multiple adsorbates could be used in the analysis, such as water vapor, hexane, and other organic vapors. Accordingly, more simulations for various adsorbates need to be carried out for the further study of nanotube structures and its properties. At the same time, the method of increasing the surface area of nanotubes and opening the pores of the tubes needs to be studied so as to improve the adsorption properties of the nanotubes. Thus the worldwide interested hydrogen storage in carbon nanotubes could be better investigated and turns the potential use to be true.

REFERENCES

REFERENCES

1. Iijima, S. Helical Microtubules Of Graphitic Carbon. *Nature* **354**, 56-58 (1991).
2. Thess, A. et al. Crystalline ropes of metallic carbon nanotubes. *Science* **273**, 483-487 (1996).
3. Dai, H.J. Carbon nanotubes: opportunities and challenges. *Surface Science* **500**, 218-241 (2002).
4. Popov, V.N. Carbon nanotubes: properties and application. *Materials Science & Engineering R-Reports* **43**, 61-102 (2004).
5. Dillon, A.C. et al. Storage of hydrogen in single-walled carbon nanotubes. *Nature* **386**, 377-379 (1997).
6. Pederson, M.R. & Broughton, J.Q. Nanocapillarity In Fullerene Tubules. *Physical Review Letters* **69**, 2689-2692 (1992).
7. Long, R.Q. & Yang, R.T. Carbon nanotubes as superior sorbent for dioxin removal. *Journal Of The American Chemical Society* **123**, 2058-2059 (2001).
8. Long, R.Q. & Yang, R.T. Carbon nanotubes as a superior sorbent for nitrogen oxides. *Industrial & Engineering Chemistry Research* **40**, 4288-4291 (2001).
9. Website of Electro-optical Systems Lab at Georgia Tech Research Institute: http://nano.gtri.gatech.edu/
10. Harris, P.J.F. Carbonaceous contaminants on support films for transmission electron microscopy. *Carbon* **39**, 909-913 (2001).

11. Endo, M. et al. Carbon Nanotubes. *Encyclopedia of Chemical Processing*, 333 - 344 (2005).

12. Agnihotri, S., Zheng, Y.J., Mota, J.P.B., Ivanov, I. & Kim, P.C. Practical Modeling of heterogeneous bundles of single-walled carbon nanotubes for adsorption applications: Estimating the fraction of open-ended nanotubes in samples. *Journal Of Physical Chemistry C* **111**, 13747-13755 (2007).

13. Liu, J.C. & Monson, P.A. Monte Carlo simulation study of water adsorption in activated carbon. *Industrial & Engineering Chemistry Research* **45**, 5649-5656 (2006).

14. Ohno, Y. et al. Chirality-dependent environmental effects in photoluminescence of single-walled carbon nanotubes. *Physical Review B* **73** (2006).

15. Yu, H., Jin, Y.G., Li, Z.L., Peng, F. & Wang, H.J. Synthesis and characterization of sulfonated single-walled carbon nanotubes and their performance as solid acid catalyst. *Journal Of Solid State Chemistry* **181**, 432-438 (2008).

16. Jeong, G.H. et al. Size control of catalytic nanoparticles by thermal treatment and its application to diameter control of single-walled carbon nanotubes. *Applied Physics Letters* **90** (2007).

17. Chen, W., Duan, L. & Zhu, D.Q. Adsorption of polar and nonpolar organic chemicals to carbon nanotubes. *Environmental Science & Technology* **41**, 8295-8300 (2007).

18. Yuan, L.M. et al. Single-walled carbon nanotubes used as stationary phase in GC. *Analytical Chemistry* **78**, 6384-6390 (2006).

19. Kang, S., Pinault, M., Pfefferle, L.D. & Elimelech, M. Single-walled carbon nanotubes exhibit strong antimicrobial activity. *Langmuir* **23**, 8670-8673 (2007).

20. Dresselhaus, M., Dresselhaus, G. & Avouris, P. Carbon nanotubes: synthesis, structure, properties and applications. (Springer, 2000).

21. Agnihotri, S., Mota, J.P.B., Rostam-Abadi, M. & Rood, M.J. Structural characterization of single-walled carbon nanotube bundles by experiment and molecular simulation. *Langmuir* **21**, 896-904 (2005).

22. Rouquerol, J. et al. Recommendations For The Characterization Of Porous Solids. *Pure And Applied Chemistry* **66**, 1739-1758 (1994).

23. Yin, Y.F., Mays, T. & McEnaney, B. Adsorption of nitrogen in carbon nanotube arrays. *Langmuir* **15**, 8714-8718 (1999).

24. Cinke, M. et al. Pore structure of raw and purified HiPco single-walled carbon nanotubes. *Chemical Physics Letters* **365**, 69-74 (2002).

25. Kong, J. et al. Nanotube molecular wires as chemical sensors. *Science* **287**, 622-625 (2000).

26. Deboer, J.H., Linsen, B.G., Vanderpl.T & Zonderva.Gj Studies On Pore Systems In Catalysts.7. Description Of Pore Dimensions Of Carbon Blacks By T Method. *Journal Of Catalysis* **4**, 649-& (1965).

27. Dubinin, M.M., Zaverina, E.D. & Radushkevich, L.V. Sorbtsiya I Struktura Aktivnykh Uglei.1. Issledovanie Adsorbtsii Organicheskikh Parov. *Zhurnal Fizicheskoi Khimii* **21**, 1351-1362 (1947).

28. Website of Wikipedia: http://en.wikipedia.org/wiki/Raman_spectroscopy.

29. Bachilo, S.M. et al. Structure-assigned optical spectra of single-walled carbon nanotubes. *Science* **298**, 2361-2366 (2002).

30. Sauvajol, J.L., Anglaret, E., Rols, S. & Alvarez, L. Phonons in single wall carbon nanotube bundles. *Carbon* **40**, 1697-1714 (2002).

31. Magee, R.W. in Rubber Division of the American Chem. Soc.1994).

32. Halsey, G. Physical Adsorption On Non-Uniform Surfaces. *Journal Of Chemical Physics* **16**, 931-937 (1948).

33. Do, D.D. Adsorption Analysis: Equilibria and Kinetics. (Imperial College Press, London; 1998).

34. New reference curve capability with the ASAP 2020 surface area and porosity analyzer from micromeritics: http:// www.azonano.com/Details.asp?ArticleID=1478.

35. Polanyi, M. Adsorption and capillarity from the stand point of the II. main clause. *Zeitschrift Fur Physikalische Chemie--Stochiometrie Und Verwandtschaftslehre* **88**, 622-631 (1914).

36. Dubinin, M.M. Fundamentals Of The Theory Of Adsorption In Micropores Of Carbon Adsorbents - Characteristics Of Their Adsorption Properties And

Microporous Structures. *Carbon* **27**, 457-467 (1989).

37. Dubinin, M.M. Chemistry and Physics of Carbon, Vol. 2. (Marcel Dekker, New York; 1966).

38. Kaganer, M.G. New Method For Determining The Specific Surface Of Adsorbents And Other Finely Divided Substances. *Zhurnal Fizicheskoi Khimii* **33**, 2202-2210 (1959).

39. Dubinin, M.M. The Potential Theory Of Adsorption Of Gases And Vapors For Adsorbents With Energetically Nonuniform Surfaces. *Chemical Reviews* **60**, 235-241 (1960).

40. Marsh, H. & Rand, B. Adverse Criticism Of Use Of T-Plot To Characterize Microporosity. *Journal Of Colloid And Interface Science* **33**, 478-& (1970).

41. Stoeckli, H.F. Microporous Carbons And Their Characterization - The Present State-Of-The-Art. *Carbon* **28**, 1-6 (1990).

42. Bansal, R.C., Donnet, J.B. & Stoeckli, H.F. Active Carbon. (Marcel Dekker, New York; 1998).

43. Siepmann, J.I. A Method For The Direct Calculation Of Chemical-Potentials For Dense Chain Systems. *Molecular Physics* **70**, 1145-1158 (1990).

44. Siepmann, J.I. & McDonald, I.R. Monte-Carlo Simulations Of Mixed Monolayers. *Molecular Physics* **75**, 255-259 (1992).

45. Frenkel, D., Mooij, G. & Smit, B. Novel Scheme To Study Structural And Thermal-Properties Of Continuously Deformable Molecules. *Journal Of*

Physics-Condensed Matter **4**, 3053-3076 (1992).

46. Depablo, J.J., Laso, M. & Suter, U.W. Simulation Of Polyethylene Above And Below The Melting-Point. *Journal Of Chemical Physics* **96**, 2395-2403 (1992).

47. Frenkel, D. & Smit, B. Understanding Modelular Simulation. (Academic Press, London; 1996).

48. Agnihotri, S., Mota, J.P.B., Rostam-Abadi, M. & Rood, M.J. Theoretical and experimental investigation of morphology and temperature effects on adsorption of organic vapors in single-walled carbon nanotubes. *Journal Of Physical Chemistry B* **110**, 7640-7647 (2006).

49. Agnihotri, S., Mota, J.P.B., Rostam-Abadi, M. & Rood, M.J. Adsorption site analysis of impurity embedded single-walled carbon nanotube bundles. *Carbon* **44**, 2376-2383 (2006).

50. Mota, J.P.B. & Esteves, I. Simplified gauge-cell method and its application to the study of capillary phase transition of propane in carbon nanotubes. *Adsorption-Journal Of The International Adsorption Society* **13**, 21-32 (2007).

51. Li, J.Y. & Zhang, J.F. A simple purification for single-walled carbon nanotubes. *Physica E-Low-Dimensional Systems & Nanostructures* **28**, 309-312 (2005).

52. Zhao, S., Shi, Z.Q., Wang, C.Y. & Chen, M.M. Structure and surface elemental state analysis of polyimide resin film after carbonization and graphitization. *Journal of Applied Polymer Science* **108**, 1852-1856 (2008).

APPENDIX

APPENDIX

Table A.1. Standard N_2 adsorption (77K) isotherm data of SWNT sample EA95, obtained from Quantachrome Autosorb-1-C equipment.

P/P_0	cm^3(STP)/g	P/P_0	cm^3(STP)/g	P/P_0	cm^3(STP)/g
1.93E-06	2.80	4.38E-04	109.19	4.16E-02	160.88
3.25E-06	5.62	5.32E-04	111.17	5.16E-02	163.25
3.78E-06	8.44	6.33E-04	113.01	6.18E-02	165.43
4.00E-06	11.26	7.38E-04	114.72	7.19E-02	167.32
4.06E-06	14.08	8.43E-04	116.29	8.20E-02	169.15
4.41E-06	48.07	9.49E-04	117.73	9.21E-02	170.76
5.13E-06	53.70	1.06E-03	119.09	1.02E-01	172.31
5.19E-06	56.52	1.16E-03	120.28	1.50E-01	178.77
5.30E-06	59.34	1.26E-03	121.36	2.00E-01	185.07
5.59E-06	62.16	1.35E-03	122.32	2.50E-01	191.45
5.97E-06	64.97	1.44E-03	123.20	3.03E-01	198.39
6.60E-06	67.79	1.52E-03	123.98	4.02E-01	211.58
7.45E-06	70.60	2.03E-03	128.21	5.01E-01	225.85
8.75E-06	73.37	2.34E-03	130.33	6.01E-01	241.54
1.08E-05	76.14	3.08E-03	134.38	7.02E-01	260.75
1.38E-05	78.89	4.10E-03	138.26	8.00E-01	287.12
1.83E-05	81.64	5.13E-03	140.98	9.00E-01	342.82
2.51E-05	84.37	6.10E-03	142.86	9.89E-01	939.41
3.52E-05	87.08	7.18E-03	144.57	9.00E-01	370.65
4.98E-05	89.77	8.29E-03	145.95	8.00E-01	302.02
6.98E-05	92.42	9.13E-03	146.86	7.01E-01	272.23
9.57E-05	95.04	1.02E-02	147.87	5.99E-01	251.01
1.28E-04	97.60	1.42E-02	151.11	4.98E-01	233.44
1.68E-04	100.10	1.71E-02	152.80	3.98E-01	216.64
2.18E-04	102.52	2.19E-02	154.94	2.98E-01	201.99
2.79E-04	104.86	2.53E-02	156.28	1.98E-01	188.06
3.53E-04	107.08	3.19E-02	158.31	9.76E-02	173.79

Table A.2. Standard N_2 adsorption (77K) isotherm data of SWNT sample CVD95, obtained from Quantachrome Autosorb-1-C equipment.

P/P_0	cm^3(STP)/g	P/P_0	cm^3(STP)/g	P/P_0	cm^3(STP)/g
1.46E-06	4.90	3.03E-04	70.76	4.17E-02	156.39
2.22E-06	7.35	3.47E-04	72.72	5.18E-02	160.50
2.75E-06	9.79	3.94E-04	74.64	6.19E-02	164.14
3.30E-06	12.23	4.44E-04	76.48	7.20E-02	167.45
3.52E-06	14.68	5.50E-04	79.98	8.21E-02	170.54
3.90E-06	17.12	6.06E-04	81.63	9.22E-02	173.47
4.18E-06	19.57	7.24E-04	84.73	1.02E-01	176.30
4.56E-06	22.01	8.47E-04	87.55	1.53E-01	188.99
5.14E-06	24.46	9.09E-04	88.86	1.99E-01	200.13
5.93E-06	26.90	1.03E-03	91.25	2.52E-01	215.76
1.09E-05	31.77	1.22E-03	94.35	3.03E-01	229.16
1.21E-05	34.21	1.54E-03	98.90	4.02E-01	255.79
1.44E-05	36.64	2.01E-03	104.15	5.01E-01	285.99
1.76E-05	39.06	2.32E-03	107.08	6.01E-01	320.52
2.16E-05	41.46	3.02E-03	112.40	7.02E-01	364.64
2.72E-05	43.86	4.02E-03	118.10	8.01E-01	425.65
3.48E-05	46.24	5.02E-03	122.44	9.02E-01	547.99
4.40E-05	48.62	6.00E-03	125.76	9.90E-01	985.21
5.57E-05	50.97	7.09E-03	128.70	8.98E-01	599.40
7.02E-05	53.31	8.02E-03	130.81	8.00E-01	449.48
8.75E-05	55.62	9.08E-03	132.84	7.01E-01	377.11
1.08E-04	57.90	1.01E-02	134.62	5.99E-01	328.44
1.32E-04	60.15	1.37E-02	138.80	4.98E-01	291.47
1.59E-04	62.36	1.70E-02	142.15	3.98E-01	256.35
1.90E-04	64.53	2.19E-02	145.99	2.99E-01	232.79
2.24E-04	66.65	2.53E-02	148.28	2.00E-01	206.44
2.62E-04	68.73	3.19E-02	152.01	1.01E-01	179.49

Table A.3. Standard N_2 adsorption (77K) isotherm data of SWNT sample CS70, obtained from Quantachrome Autosorb-1-C equipment.

P/P_0	cm^3(STP)/g	P/P_0	cm^3(STP)/g	P/P_0	cm^3(STP)/g
1.51E-06	6.19	2.01E-04	122.93	4.14E-02	234.41
2.25E-06	9.27	2.33E-04	125.54	5.15E-02	239.89
2.76E-06	12.35	3.08E-04	130.56	6.17E-02	244.77
2.89E-06	15.43	3.99E-04	135.31	7.18E-02	249.23
3.15E-06	18.51	5.03E-04	139.73	8.19E-02	253.28
3.26E-06	24.67	6.21E-04	143.81	9.20E-02	257.08
3.42E-06	27.75	7.45E-04	147.52	1.02E-01	260.62
3.49E-06	30.83	8.08E-04	149.25	1.52E-01	276.02
3.68E-06	40.08	9.39E-04	152.42	2.03E-01	289.40
4.20E-06	49.39	1.01E-03	153.90	2.53E-01	303.04
5.04E-06	55.55	1.20E-03	157.80	3.02E-01	320.01
5.71E-06	58.62	1.54E-03	163.49	4.01E-01	348.42
6.46E-06	61.69	2.02E-03	169.80	5.00E-01	379.46
8.17E-06	67.75	2.33E-03	173.33	6.00E-01	415.14
9.59E-06	70.77	3.04E-03	179.62	7.02E-01	461.33
1.52E-05	79.80	4.04E-03	186.09	8.01E-01	527.58
1.84E-05	82.80	5.02E-03	190.93	8.99E-01	666.95
2.21E-05	85.79	6.10E-03	195.10	9.91E-01	1091.54
3.13E-05	91.73	7.04E-03	198.02	9.00E-01	771.13
4.47E-05	97.63	8.07E-03	200.76	7.98E-01	544.36
5.36E-05	100.56	9.12E-03	203.20	6.99E-01	470.44
6.41E-05	103.46	1.02E-02	205.42	5.99E-01	424.82
7.65E-05	106.34	1.36E-02	210.84	4.96E-01	394.33
9.08E-05	109.20	1.69E-02	215.17	3.99E-01	354.40
1.07E-04	112.02	2.17E-02	220.17	2.98E-01	323.88
1.26E-04	114.81	2.52E-02	223.33	1.98E-01	294.28
1.48E-04	117.56	3.17E-02	228.40	1.00E-01	263.51

Table A.4. Standard N_2 adsorption (77K) isotherm data of SWNT sample BU90, obtained from Quantachrome Autosorb-1-C equipment.

P/P_0	cm^3(STP)/g	P/P_0	cm^3(STP)/g	P/P_0	cm^3(STP)/g
1.83E-06	2.10	3.61E-04	55.41	4.03E-02	134.71
3.20E-06	4.21	3.92E-04	57.09	5.04E-02	138.49
4.13E-06	6.32	4.25E-04	58.74	6.06E-02	141.91
4.91E-06	8.43	4.58E-04	60.36	7.08E-02	145.11
6.01E-06	10.54	4.93E-04	61.94	8.09E-02	148.10
7.65E-06	12.64	6.04E-04	66.48	9.10E-02	151.00
1.04E-05	14.74	7.25E-04	70.67	1.01E-01	153.79
1.39E-05	16.83	8.12E-04	73.26	1.51E-01	166.95
1.87E-05	18.92	9.01E-04	75.68	2.01E-01	179.63
2.47E-05	20.99	9.96E-04	77.94	2.51E-01	192.63
3.18E-05	23.07	1.23E-03	82.82	3.02E-01	208.66
4.50E-05	25.12	1.51E-03	87.20	4.00E-01	238.14
5.18E-05	27.17	2.03E-03	93.08	5.02E-01	271.15
6.17E-05	29.19	2.33E-03	95.69	6.01E-01	307.82
7.36E-05	31.19	3.02E-03	100.01	7.02E-01	355.61
8.72E-05	33.17	4.05E-03	104.47	7.99E-01	423.91
1.02E-04	35.14	5.10E-03	107.70	9.89E-01	1313.09
1.19E-04	37.10	6.10E-03	110.11	9.01E-01	638.15
1.37E-04	39.03	7.03E-03	111.91	8.00E-01	466.44
1.56E-04	40.95	8.10E-03	113.66	7.00E-01	379.86
1.77E-04	42.84	9.22E-03	115.21	5.97E-01	322.31
1.99E-04	44.71	1.03E-02	116.59	4.99E-01	280.33
2.23E-04	46.56	1.37E-02	120.15	3.98E-01	239.19
2.48E-04	48.39	1.65E-02	122.45	2.98E-01	208.76
2.79E-04	50.18	2.10E-02	125.50	1.98E-01	180.83
3.03E-04	51.95	2.46E-02	127.60	1.00E-01	154.46
3.31E-04	53.69	3.09E-02	130.74		

VITA

Yijing Zheng was born in Zhengzhou, China on February 18, 1983. She was raised in Hangzhou, Zhejiang Province. She graduated from the Hangzhou No. 2 Middle School in 2002. From there, she went to Zhejiang University of Technology and received her bachelor's degree in environmental engineering in 2006 in Hangzhou. She came to the University of Tennessee, Knoxville and joined the Department of Civil and Environmental Engineering in August of 2006. She earned her M.S. degree in Environmental Engineering from the University of Tennessee in 2008. During her graduate studies at Knoxville, Yijing has published three peer reviewed journal articles and contributed in writing one research proposal. Before the time she graduated, she had been accepted into the Ph.D. program in Chemical Engineering at the University of Pittsburgh, PA.